UNIVERSITAT DE LES
ILLES BALEARS

Master Thesis

OPTICAL COMMUNICATIONS USING CHAOTIC CARRIERS GENERATED BY ELECTRO-OPTICAL FEEDBACK DEVICES

Author:
Romain Modeste
NGUIMDO

Supervisor:
Pere
COLET RAFECAS

October 7, 2008

OPTICAL COMMUNICATIONS USING CHAOTIC CARRIERS GENERATED BY ELECTRO-OPTICAL FEEDBACK DEVICES

Romain Modeste NGUIMDO

Acknowledgments:

This work is the Thesis for the Master in Physics of the Universitat de les Illes Balears, and it has been done thanks to the program "Formación de personal de investigación" (FPI).

I would like to express my gratitude to:

- The Spanish Government, as well as the University of Balearic Islands.
- Prof. Pere Colet for the supervision of this work and his dedicated attention to me. I will never forget his entire disponibility and implication for this work. Thanks to him I have never felt far of my family and my country.
- The staff of IFISC for their help and the nice working environment that they create.
- Professors Maxi San Miguel, Claudio Mirasso, Raúl Toral, Emilio Hernández-García and Víctor M. Eguíluz for their teachings and advices for my integration in Palma and IFISC.
- Prof. Paul Woafo for his always valuable teachings and for his fruitful advices
- Dr. Yanne Chembo Kouomou for trusting in my capabilities.
- Adrian Jacobo for sharing with me so many good moments, and for his help with my research.

Contents

Chapter 1

Introduction

Since the development of telecommunications there is an ever growing interest in finding more secure ways to send the information. A possible way to do this is using the **Vernam cipher**[1] which is based on digital information (strings of N binary data.) where any analogic signal is first digitalized. Subsequently the digitalized message is convoluted with a given binary pattern (the key composed also of N binary data) so that it is scrambled and an eavesdropper cannot recover the message. The key is supposed to be known by the sender of the message and the new binary string is safely sent in a public communication channel [2]. Usually, the sender transmits this key to the addressee who uses to recover the original message by deconvoluting the sent message. Thus, with this technique, an eavesdropper has 2^N possible messages and it is more difficult to know which is the original one.

However, it is not suitable for secure communications between two persons who do not know each other: it is not accordingly suitable for the business operations and digital signature. Furthermore, it is very constraining for very long messages since the code is long as the message and therefore demands larger physical space to be kept. On the other hand the key should be used only once. Thus all the efforts deployed to keep the key secret are inverted for the transmission of a single message. To circumvent the drawbacks of the **Vernam cipher**, other software cryptosystems have been developed, and the most popular is the so-called RSA algorithm proposed by **Ron Rivest, Adi Shamir** *and* **Len Adelman** in 1978 [3]. This algorithm generates two keys, one public and one private so that two persons who did not know each other before can communicate securely. Nowadays, the growing of technology performance threatens current techniques used to secure the communications. For example in 1994, the american scientist **Peter Shor** developed an algorithm which may potentially crack any ciphertext (convoluted message) encripted with a public key algorithm, mainly the short message [4]

To get around these drawbacks, people developed an alternative way of encryption relying on chaos. Before that the chaos was useful in the understanding

of some phenomenons in biology, chemistry, physics, etc... But its most exciting in lasers goes back to the pioneering works of Haken in 1975 [5] who implemented the possibility of chaotic behaviour in lasers. It has proven that when a system presents both nonlinearity and complex enough phase space, it can lead to chaotic behaviour. Subsequently, the chaotic behaviour has encountered in almost all types of lasers (solid-state [6], gas ring [7], semiconductor [8], etc...).

This last decade, the chaos has utilized to cryptography and the key lies on synchronization of chaotic carriers used to encode the message. The first synchronization of chaotic carriers was proposed by **Pecora** *and al.* in 1990 [9] and the first chaos based on communications was done with the electronic circuits by **Cuomo** *and al.* in 1993 [10]. Subsequently, several investigations have dealt with chaos cryptography by synchronizing fiber ring lasers [11, 12], semiconductor lasers [13, 14, 15, 16] and microchip lasers [17] with applications in communications using optical fibers and those based on semiconductor lasers. In the concept of chaos encryption, high-quality synchronization of chaos in the transmitter and receiver lasers is required to recover the hidden message. This synchronization is facilitated when the receiver is similar enough to the emitter. In addition, synchronized chaotic carriers could be used in the technique explained before for generating correlated random signals to obtain secret keys which are secure in the sense of information theoretic security [18, 19]. When the message is encoded within the chaotic carrier, a possible eavesdropper cannot distinguish the message from the chaos. The security of chaos cryptography also demands that the message to be encoded should be small compared to the chaotic carrier. Even though the eavesdroppers try to build a chaotic receiver identical to the emitter, they would have to face the parameter mismatch problem which impedes the proper extraction of the message

The first chaotic communication schemes have shown vulnerable to be attacked because of the narrow spectra of the chaos used. Thus, another method for communicating by chaos has been reported. It relies on nonlinear optical delayed feedback systems. **Ikeba** obtained the chaos using semiconductor lasers with delay [20]. Along the same line, **Lang** and **Kobayashi** proposed similar device where a fraction of the delayed output radiation of a semiconductor laser is fed back into the active region layer [21] . Subsequently, the introduction of both (feedback+parameter modulation) has proven to be useful in the optical systems where chaos cryptography was first theoretically proposed [22]. The first experimental demonstration was built in 1998, by **Van Wiggeren and Roy** using erbium-doped fiber ring-lasers [23, 24], and by **Larger** *et al.* using the chaos generated by a semiconductor laser [25, 26]. Some of its properties have been theoretical and experimentally investi-

gated by **Chembo** *and al.*[27, 28, 29]

In this report, we review the properties of this last system and explore another scheme involving the combination of electro-optical elements which consists in injecting back a fraction of the signal in the laser serves as a light source. It is organized as follows:

- In chapter II, we present the semiconductor laser with electro-optical feed back loop,
- In chapter III, we deal with new model of semiconductor lasers subjected to feedback pump current: linear and nonlinear in feedback carrier will be explored.
- Chapter IV is devoted to the conclusion and future work.

Chapter 2

Semiconductor lasers with electro-optical feedback

Generally, electro-optical systems are a combination of electronic and electro-optical components such as light emitting diodes, image intensifiers, and lasers. Examples of such devices are the night vision goggles and rifle sights, laser range finders, markers and designators, and forward looking infrared receivers. However, all the electro-optical devices need some source of light to produce an image of an object through illumination, amplification, or thermal imaging. Most of the devices use lasers as the light source because of their low running threshold.

The lasers are also associated with electro-optical elements for the production of chaotic carriers. One way to do that consists in embedding a resonator and electro-optical feedback through the Mach-Zehnder modulator and pump this with semiconductor laser. With this device, we can distinguish two main blocks: The first is the light source which involves the laser and the second is the feedback loop. In this chapter, we first briefly describe the dynamics of the semiconductor (SC) laser. Secondly, we introduce an electro-optical loop to produce chaotic behaviour. Then we will show how this chaos can be used to encode the message whose decoding is also performed in the conditions which are described by the end of the chapter.

2.1 Semiconductor laser

2.1.1 Principles of photon emission

There is a wide variety of lasers (solid state-, gas-, dye-, and fiber-lasers, etc...). All these lasers are composed by the same elements: Lasing material (crystal, gas, etc...), an optical cavity, power source. Among the variety of lasers, the most widespread ones are the semiconductor lasers because of their large range of wavelengths, coupled to the wide variety of structures. In addition, they are compact and cheap, and they are used in many devices like CDs, DVDs, optical communications, etc... They

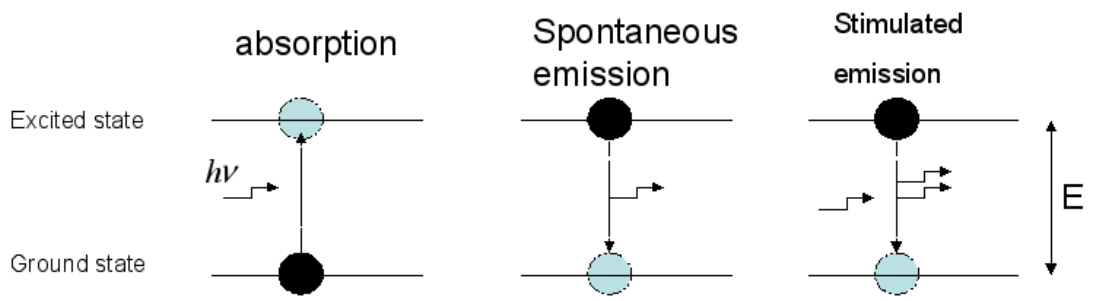

Figure 2.1: illustration of 3 mechanisms of photon interaction with 2 level system

can also be associated in array configurations to produce high-power laser sources which are used to drill and cut, or to pump other types of lasers. SC lasers operate with the principle of doping which is characterized by the extra-electrons coming from forward electrical bias which causes two species of charge carrier: holes with positive charge and electrons with negative charge. The performance depends on the base material and the widespread ones are silicon and gallium.

Lasers operate by the principle of stimulated emission. Electrons in the atoms of the lasing material reside in a steady-state. When energy is pumped into an atom, its electrons are excited to the higher energy level which is unstable (Fig.2.1, absorption). The electrons will stay in this state for a short time and then decay back to their original energy state. This decay occurs in two ways:

- Spontaneous decay: When an electron and a hole are present in the same region, they may recombine or "annihilate" with the result being spontaneous emission i.e., the electron may reoccupy the energy state of the hole, emitting a photon with energy equal to the difference between the electron and hole states involved. Hence, the electron simply falls to their ground state while emitting randomly directed photons (Fig.2.1, spontaneous emission). Spontaneous emission is necessary to initiate laser oscillation.

- Stimulated decay: In the absence of stimulated emission (i.e., lasing) conditions, electrons and holes may coexist in proximity to one another, without recombining, **for a certain time** (named the "upper-state lifetime" or "recombination time," of about a nanosecond for typical diode laser materials before they recombine. If the atom is in this state, a nearby photon with energy equal to the recombination energy can cause recombination by stimulated emission. This generates another photon of the same frequency, travelling in the same

direction, with the same polarization and phase as the first photon: coherent photon (Fig.2.1, stimulated emission). This means that stimulated emission causes gain in an optical wave (of the same wavelength) in the injection region, and the gain increases as the number of electrons and holes injected across the junction increases.

The second ingredient of a laser is the resonator. The light is amplified in a cavity resonator also known as an optical cavity, which is usually composed of two or more mirrors. This will allow standing wave modes to exist with little loss. There are many kinds of resonators: klystron tube waveguide with at least two apertured cavity resonators and the reflex klystron utilizing only a single apertured cavity resonator through which the beam of charged particles passes.

2.1.2 Modelization of the semiconductor laser

The semiconductor laser (SC) with constant frequency can be described by the rate equations in terms of the number of photons I and the carrier number N inside the active layer [30]

$$\frac{dI}{dt} = (G-\gamma)I + 4kN + \sqrt{4kNI}\zeta(t) \tag{2.1}$$

$$\frac{dN}{dt} = J_0 - \gamma_e N - GI \tag{2.2}$$

$$G = g_m(N-N_0)/(1+sI) \tag{2.3}$$

The carrier lifetime $1/\gamma_e$ is defined as the average time it takes an excess of carriers to recombine; the photons lifetime $1/\gamma$ is a time constant that describes the decay (or the growth) of energy in a cavity; g_m is the gain parameter; N_0 is the carrier number at transparency; k is the amplitude of noise and the J_0 the injected current: The behaviour of the laser mostly depends on the excitation density (injection current). If the material is not excited enough, the number of carriers in the excited state is weak and then the absorption probability is greater than the probability of emission. However, when we increase the injected current, the number of carriers in the excited state grows and beyond a threshold (called threshold current), the recombination probability by stimulated emission is greater than the absorption one and therefore, the laser starts to lase.

In eqs.(2.3), the gain saturation factor given by $(1+sI)$ is included in [31] to summarize a set of physical effects that eventually bound the material gain as the number of intracavity photons is increased. Thus, the laser cannot have an infinite gain for any value of the injected current. The term $4kN$ is the mean photon

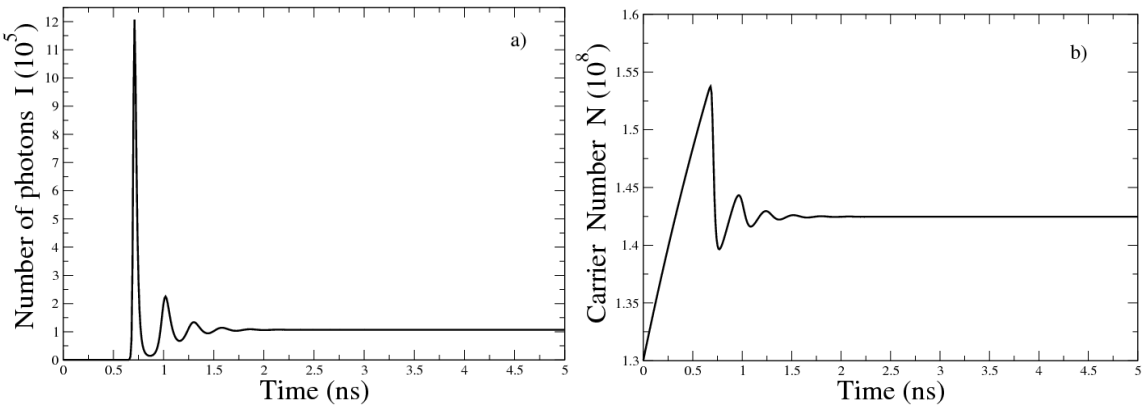

Figure 2.2: Evolution of the number of photons (a)) and carrier(b)) in time with parameters given in Table 1

number emitted by spontaneous emission while the term $\sqrt{4kNI}\zeta(t)$ stands for the fluctuations around this mean photon number. The noise is considered to be white Gaussian . We have neglected the effect of the radioactive and nonradioactive carrier generations and the noise recombination of the carrier number since it is negligible compared with the fluctuations induced by the noise on the number of photons I [32, 33].

To simplify the study, let us consider the ideal case which corresponds to the absence of spontaneous emission ($k = 0$). Thus, the random processes (spontaneous emission and fluctuations) are eliminated. The rate equations become

$$\frac{dI}{dt} = (G - \gamma)I \tag{2.4}$$

$$\frac{dN}{dt} = J_0 - \gamma_e N - GI \tag{2.5}$$

The steady state for N and I is obtained when $\frac{dI}{dt} = \frac{dN}{dt} = 0$. The minimum current beyond which all the losses (absorption, etc...) are compensated is obtained for $I = 0$ and $G = \gamma$ i.e., $J_{th} = \gamma_e N_{st} = \gamma_e(\frac{\gamma}{g_m} + N_0)$. According to the injected current, one can distinguish two different regimes :

- $J_0 < J_{th}$: In this case, the gain is less than the losses and thereby no power is delivered at the output of the laser (I=0). The steady state is given by $I = 0$, i.e., $(I_{st} = 0, N_{st} = J_0/\gamma_e)$. This stationary point is unprofitable in practice because the laser has no output , however, it allows us to the undertanding of the laser dynamics.

- $J_0 > J_{th}$: In this case, the gain is greater than the losses and therefore there is an optical power of the laser. The stationary state is obtained when $G = \gamma$, $I > 0$ i.e.,

$$I_{st} = \frac{J_0 g_m - \gamma_e g_m N_0 - \gamma_e \gamma}{\gamma(g_m + s\gamma_e)} \tag{2.6}$$

$$N_{st} = \frac{g_m N_0 + \gamma + sJ_0}{g_m + s\gamma_e} \tag{2.7}$$

  It is important to remark that the difference between N_{st} and N_{th} is only due to the gain saturation effects. Hence if $s = 0$ then $N_{th} = N_{st}$ but $I_{th} = 0$ whereas $I_{st} > 0$.

In the following, we address in the performance of the laser when it operates above the threshold. We work with the parameters compatible with the experiment as written in Table 1 [34].

Table 1: laser parameters

Parameter	**Meaning**	**Value**	**Units**
g_m	gain parameter	$1.5X10^{-8}$	ps^{-1}
s	gain saturation factor	$2X10^{-7}$	adimensional
N_0	carrier number at transparency	$1.2X10^{8}$	adimensional
γ	inverse photon lifetime	$3.3X10^{11}$	s^{-1}
γ_e	inverse carrier lifetime	$5X10^{8}$	s^{-1}
J_{th}	threshold current	$7.1X10^{16}$	s^{-1}
J_0	injection current	$J_0 = 1.5J_{th}$	s^{-1}

With our parameters, $J_{th} = 7.1X10^{16}s^{-1}$ and fixing $J_0 = 1.5J_{th}$, we plot the time traces of N and I starting with $I = 10^2$ photons and $N = 1.3X10^8$ carriers in the active layer in Fig.(2.2). The observed oscillations called "relaxation oscillations "are due to the intrinsic frequency of the laser which is in the order of $10GHz$. In fact, there is a time during which the injection current is changed from the threshold to a constant value above the threshold. After this time, the laser relaxes to steady-state conditions. After this transient regime, it goes to the stable stationary lasing state given by eqs. (2.6) and (2.7). Using the parameters stated in Table 1, we have $N = 1.42X10^8$ and $I = 1.068X10^5$ which are in good agreement with the numerical results shown in Fig.(2.2) after the transient time.

Eqs. (2.6) and (2.7) predict that semiconductor lasers are not chaotic. Typically ways to induce chaos are:

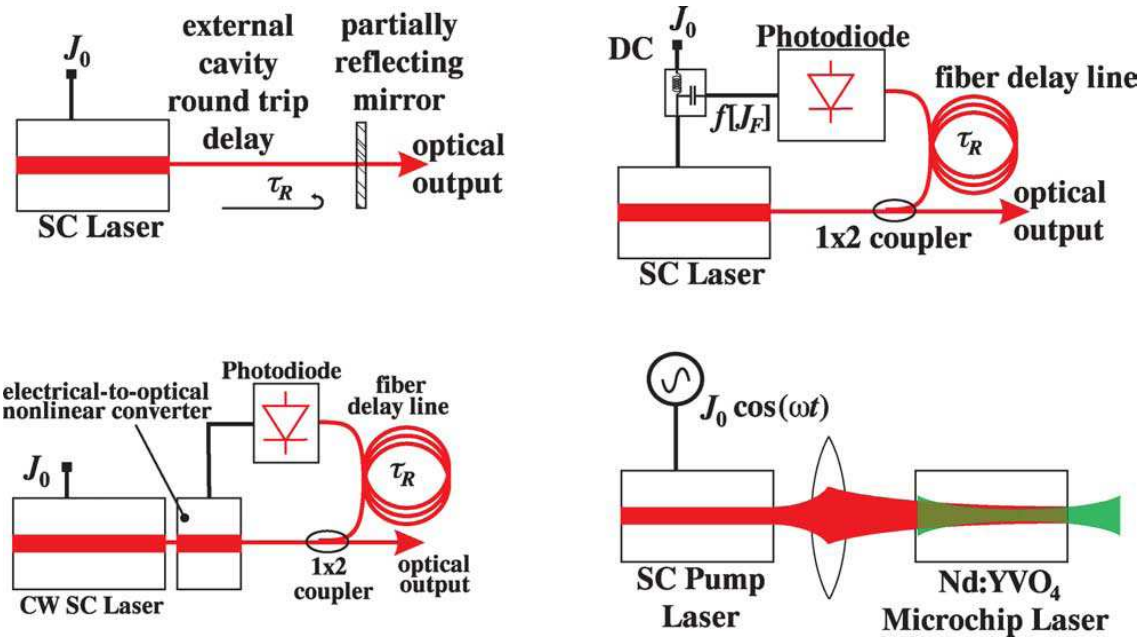

Figure 2.3: Four sub-class of nonlinear dynamics in Optics mostly involved in optical chaos generation for encryption (Figure taken from ref.[35]).

♣ To add an optical feedback: the external cavity lasers (see Fig.2.3, upper left) can involve linear feedback delay terms. In this case, the nonlinear operation consists in a coupling in the rate equations between the optical field amplitude and the inversion population density.

♣ To add a system with electro-optical feedback: In this case, the delayed feedback has two main properties: it is nonlinear, and it is optical phase insensitive due to the electronic nature of the feedback. This situation can be explored in two distinct schemes. In the first one (Fig. 2.3, upper right), the lasing process still originates from the laser rate equations, in which the nonlinear coupling between the inversion population density and the optical field amplitude involves a delay term originating from the feedback signal acting on the electronic pumping strength. In the second case (Fig. 2.3, lower left), the lasing process is determined by the linear filtering performed by the electronic part of the oscillator feedback; this filtering is applied to a scalar nonlinear feedback transformation. This latter case is briefly detailed in this work.

♣ Modulating the injection currentJ_0: It involves nonlinear coupled rate equa-

tions in a solid state laser between population inversion and the optical electric field, when the population inversion is driven by an externally modulated pump laser (see Fig. 2.3, lower left).

2.2 The feedback loop

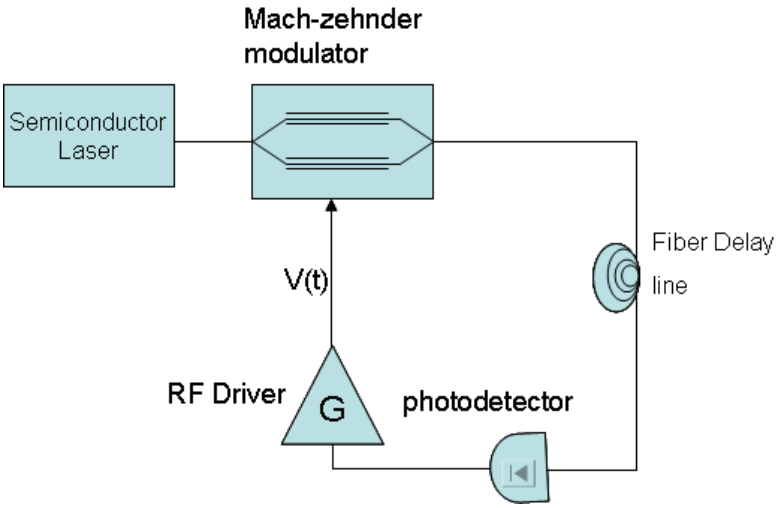

Figure 2.4: setup of semiconductor laser with one electro-optical feedback

In this section, we focus on the basic setup of Fig.(2.3, lower left) and we choose the Mach-Zehnder modulator as our electro-optical device. The architecture is brought together in the setup shown in Fig.(2.4) made up as follows:

- A continuous-wave (CW) semiconductor laser delivering a constant power P which is proportional to the number of photons I: $P = k_1 I$. The proportionality coefficient is $k_1 = h\nu$ where h stands for Planck constant while ν is the emission frequency of the photon.

- The Mach-Zehnder modulator: a Mach-Zehnder is an interferometer with two inputs of which one is an optical signal and other an electrical. Its main property consists in dividing ideally the input light beam into two light beams and recombining it at the output. Thus, when the voltage V is applied in the transverse direction of one arm, its refractive index changes almost linearly. This difference of index generates a phase-shift on the light propagating on that arm

and then interferes with the light coming from the other arm. Therefore, the incoming light P is modulated during the recombination at the output in such away that the output power is $Pcos^2(\frac{\pi}{2}\frac{V}{V_\pi})$ where V_π is called half-wave voltage and it corresponds to the voltage needed to impose a π phase-shift. The Mach-Zehnder modulator has two components involving the voltage: a constant or DC (direct current) component V_B that serves to select the operating point of the modulator; and a RF (radio-frequency) component $V(t)$ which ensures nonlinear dynamics operations. Therefore, the output of the Mach-Zehnder modulator can be rewritten as $Pcos^2(\frac{\pi}{2}\frac{V(t)}{V_{\pi RF}} + \frac{\pi}{2}\frac{V_B}{V_{\pi DC}})$ where $V_{\pi RF}$ and $V_{\pi Dc}$ stand for the RF half-wave and the bias electrode half-wave respectively.

- A fiber delay line used to shift the optical signal in time with a delay T
- An amplified diode which detects and converts the optical signal into the electrical one with sensitivity s.
- Radio-Frequency (RF) driver which is a linear filter with a gain G whose electrode is applied directly to Mach-Zehnder. This linear filter is modeled by a second-order bandpass filter with a low cutoff response time f_L and the high cutoff frequency f_H. The bandpass filter is made up of a low-pass filter whose output voltage $U(t)$ is related to the input $U_1(t)$ by the first order differential equation as follows

$$U_1(t) = \frac{1}{2\pi f_L}\frac{d}{dt}U(t) + U(t) \tag{2.8}$$

and a high-pass filter for which the output is related to the input by $U_2(t)$ is

$$U(t) = 2\pi f_H \int_{t_0}^{t} U_2(t)ds + U_2(t) \tag{2.9}$$

The combination of eqs.(2.8) and (2.9) leads to

$$U_1(t) = (1 + \frac{f_L}{f_H})U_2(t) + \frac{1}{2\pi f_L}\frac{d}{dt}U_2(t) + 2\pi f_H \int_{t_0}^{t} U_2(t)ds \tag{2.10}$$

On the other hand, the output voltage $V(t)$ amplified with the RF gain G is proportional to the output voltage $U_2(t)$ of the high-pass filter: $V(t) = gGU_2(t)$. Then it modulates the optical power of the semiconductor laser which subsequently, is delayed in time travelling the optical fiber and finally arriving at the photodetector with sensitivity s before being used as the input in low-pass filter:

$U_1(t) = gGsk_1Icos^2(\frac{\pi}{2}\frac{V(t-T)}{V_{\pi RF}} + \frac{\pi}{2}\frac{V_B}{V_{\pi DC}})$.
In terms of the radio-frequency voltage $V(t)$, we have

$$(1+\frac{f_L}{f_H})V(t) + \frac{1}{2\pi f_L}\frac{dV(t)}{dt} + 2\pi f_H\int_{t_0}^{t} V(t)ds = gGsk_1Icos^2(\frac{\pi}{2}\frac{V(t-T)}{V_{\pi RF}} + \frac{\pi}{2}\frac{V_B}{V_{\pi DC}}) \quad (2.11)$$

we take the advantage that $f_L \ll f_H$ and introducing the dimensionless variable $X(t) = \frac{\pi V(t)}{2V_{\pi RF}}$, then we have

$$x + \tau\frac{dx}{dt} + \frac{1}{\theta}\int_{t_0}^{t} x(s)ds = \beta_1 I\cos^2[x(t-T)+\phi], \quad (2.12)$$

with the parameters defined in Table 2. The overall normalized electro-optical oscillator gain $\beta = \beta_1 I$.

Table 2: electro-optical loop parameters

Parameter	**Meaning**	**Value**	**Units**
$\tau = 1/2\pi f_H$.	high cutoff frequency	25	ps
$\theta = 1/2\pi f_L$	low cutoff response time	5	μs
$\beta_1 = \pi gsGk_1/2V_\pi$	normalized electro-optical gain coefficient	2.89X10^{-5}	adimensional
$\phi = \pi V_B/2V_{\pi_{DC}}$	off-set phase	$0 \le \phi \le 2\pi$	rads
T	delay time	2.5	ns

2.3 Theoretical and numerical study

In this section, we work with the numerical values stated in Table 1 and 2, and compatible with those of experiment in [27]. We take ϕ as the control parameter and we study the effects of the injection current as well. Because I and N are constant after the transient time as we showed in Fig.(2.2), the normalized electro-optical gain $\beta = \beta_1 I$ is constant and can be considered as a parameter. In this case, I is given by the relation (2.6).

Eq. (2.12) can be rewritten letting $w = \int_{t_0}^{t} x(s)ds$ as a pair of equations such as follows

$$x + \tau\frac{dx}{dt} + \frac{1}{\theta}w = \beta_1 I\cos^2[x(t-T)+\phi] \quad (2.13)$$

$$\frac{dw}{dt} = x \quad (2.14)$$

When $\frac{dx}{dt} = \frac{dw}{dt} = 0$ there is a fixed point that is $(x_s = 0, w_s = \theta\beta\cos^2\phi)$. Taking $x = x_s + x_1$ and $w = w_s + w_1$, linearizing eq. (2.13) around the fixed point and

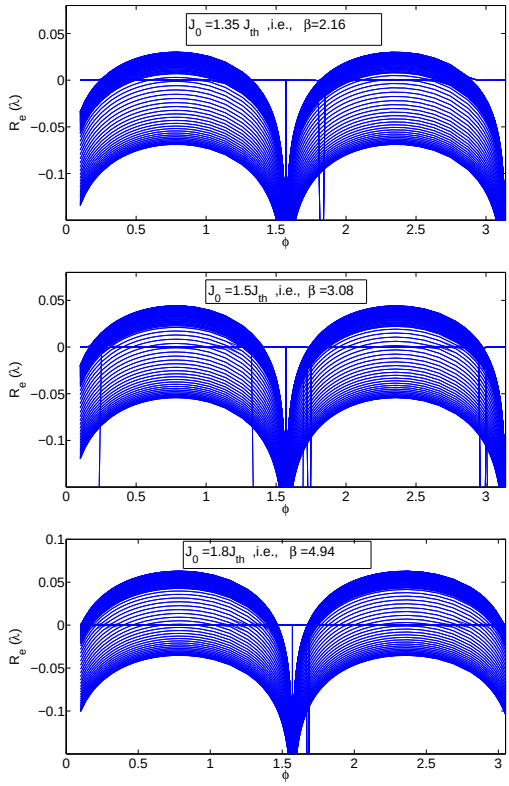

Figure 2.5: Real part of solutions given by the eigen equation versus off-set phase

taking into account eq.(2.14) we obtain

$$x_1 + \tau\frac{dx_1}{dt} + \frac{1}{\theta}w_1 = -\beta \sin 2\phi x_1(t-T) \tag{2.15}$$

$$\frac{dw_1}{dt} = x_1 \tag{2.16}$$

Assuming $x_1 \sim e^{\lambda t}$ and $w_1 \sim e^{\lambda t}$ we investigate the stability of the fixed point through 2 by 2 matrix with eigen equation given by

$$\text{detM}= \begin{vmatrix} -\lambda - \frac{1}{\tau} - \frac{\beta}{\tau} sin(2\phi)e^{-\lambda T} & -\frac{1}{\tau\theta} \\ 1 & -\lambda \end{vmatrix} = 0$$

where λ are the eigenvalues. From this determinant, we have.,

$$\lambda^2 + \lambda(\frac{1}{\tau} + \frac{\beta}{\tau} sin(2\phi)e^{-\lambda T}) + \frac{1}{\tau\theta} = 0 \tag{2.17}$$

The system is stable if and only if all the real part of λ are negative; otherwise it is unstable. The computation of the eq.(2.17) can be done using Netwon-Raphson

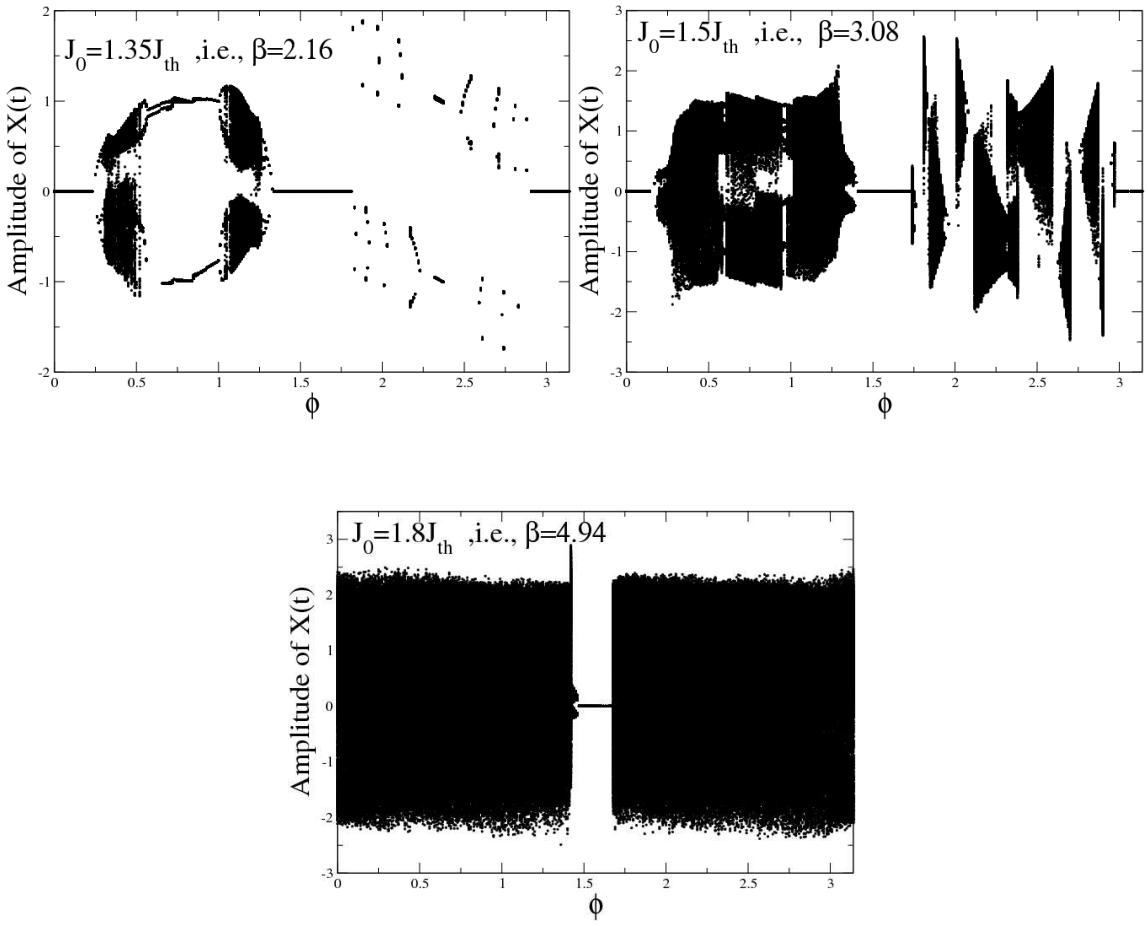

Figure 2.6: Bifurcation diagram versus off-set phase ϕ for different injection currentJ_0

method. Because of the term $e^{-\lambda T}$, eq.(2.17) can have an infinite number of solutions. A practical way to find the stability is to compute eq.(2.17) using DDE-BIFTOOL algorithm in matlab [36]. The presence of $sin2\phi$ in eq.(2.17) shows that the function is $\pi - periodic$ and thereby we can restrict the stability analysis only over a range of π. Fig.(2.5) shows the real part $R_e(\lambda)$ of λ with respect to the values of offset phase ϕ and the injected current.

♠ For $R_e(\lambda) < 0$, the fixed point is stable (steady state). This occurs for some values of the phase. This behaviour is due to the fact that in the interferometer the phase-shift provokes in some points destructive effects and constructive effects in some others. In fact, the input light beam is ideally divided in two equal parts inside the interferometer but only the light beam of the arm where the voltage has been applied undergoes the phase modulation whereas the second beam only suf-

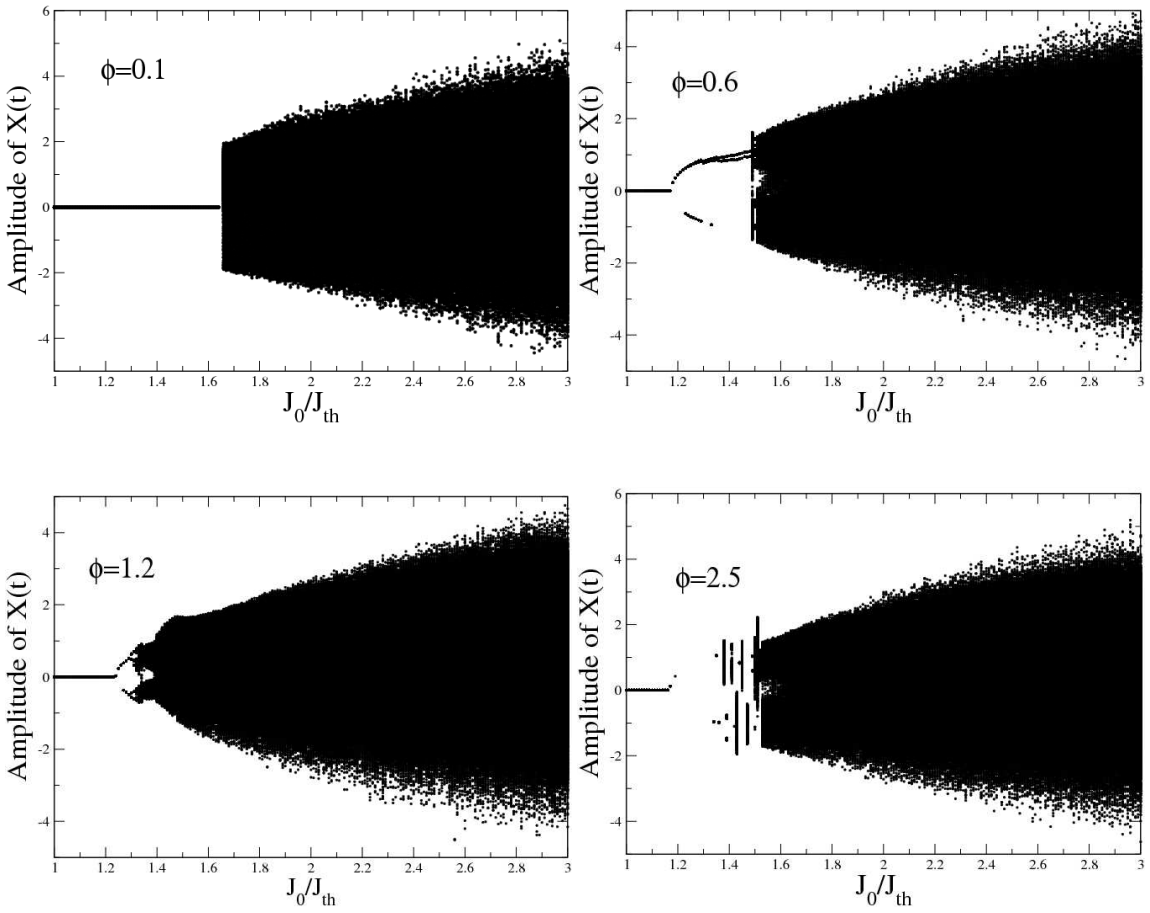

Figure 2.7: Bifurcation diagram versus injection current J_0
for different values of the off-set phase ϕ

fers the material phase-shift. Thus, when the two light beams interfer during the recombination at the output, they mutually destroy if the phase difference is $\pi/2$. In Fig.(2.5, top), the stability shows three domains of steady state: the system is stable for the values of phase belonging to $\phi \in [0, 0.25] \cup [1.3; 1.8] \cup [2.9; \pi]$. When one increases the injected current to $J_0 = 1.5J_{th}$, each stable area becomes more narrow. We notice for $J_0 = 1.8J_{th}$ that the steady states have disappeared for the small values of phase and those close to π but it remain around $\pi/2$

♠ For the offset phase values given $R_e(\lambda) > 0$, the system is unstable. We can collect information on the unstable area by plotting the bifurcation diagram. All the results are performed after integrating over a time of $80\mu s$ which is *16 times* longer than the slowest scale of the model θ. The time step used for the numerical simulations is $1ps$. We deal with the parameters of the laser and the feedback loop

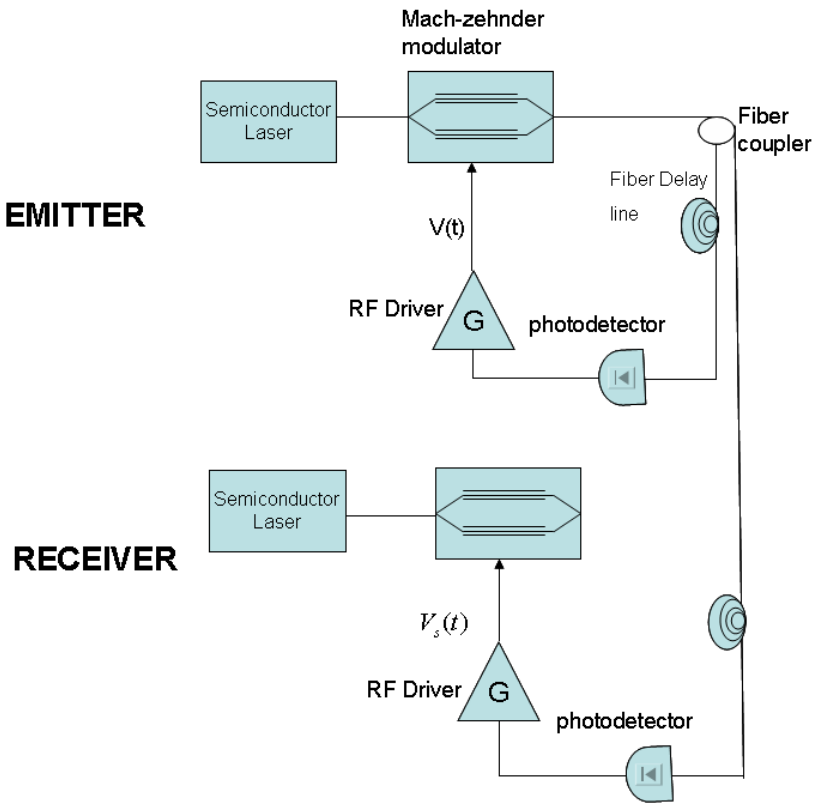

Figure 2.8: synchronization setup

which are easy to measure in experiments, i.e., offset phase for feedback loop and the injection current for the laser. Because of the $\cos^2()$ term in eq.(2.13), ϕ is equivalent to $\phi + \pi$. Thus it is reasonable to explore the effects of phase by analyzing the bifurcation diagram only over a range of π. Fig.(2.6) shows steady states in good agreement with those found by the stability analysis. For $\beta = 2.16$, the first unstable area shows narrow band chaos alternating with oscillations depending on the value of ϕ. The transition from the steady state to the chaos or vice versa passes through period doubling. The second unstable area shows non-stationary dynamics. If β is increased to $\beta = 3.08$, this area becomes chaotic while the first unstable one becomes ever more chaotic and further increasing the injected current, all the non-stationary areas become chaotic as it is seen with $\beta = 4.94$.

The change of the injected current is necessary in experiments where it is tuned to observe different dynamical regimes such as the chaotic one. The bifurcation diagram plotted in Fig.(2.7) shows how J_0 can induce chaos . Thus, one notices

that J_0 should be large compared with J_{th} to induce instability in the filter loop. For small values of ϕ, the system moves directly from the steady state to chaos (see Fig.(2.7, top-left)) while it passes through a Hopf bifurcation or period doubling before becoming chaotic for slightly large ϕ (see Fig.(2.7), for $\pi = 0.6$; 1.2 or 2.5). As it is seen in Fig.(2.7), it is necessary to take at least $J_0 > 1.6J_{th}$ corresponding to $\beta = 3.7$ to have the chaotic regime required for encryption. The key of the decryption lies on the synchronization of the chaotic carrier with the receiver.

2.3.1 Synchronization of two electro-optical semiconductor lasers with electro-optical feedback

We consider two separate electro-optical systems consisting in one with closed loop namely emitter and other with open loop which is forced by the signal coming only from the transmitter (receiver). The receiver (slave) is built similarly to the emitter (master). The schematic setup of the coupled master-slave system is exhibited in Fig.(2.8) and its dynamics is described by the set of equations

$$\begin{cases} x + \tau\frac{dx}{dt} + \frac{1}{\theta}\int_{t_0}^{t} x(s)ds = \beta_1 I\cos^2[x(t-T)+\phi] \\ y + \tau_s\frac{dy}{dt} + \frac{1}{\theta_s}\int_{t_0}^{t} y(s)ds = \beta_{1s} I_s\cos^2[x(t-T_s)+\phi_s] \end{cases} \quad (2.18)$$

where the subscript "s" denotes the receiver and $y(t) = \frac{\pi V_s(t)}{2V_{\pi RF}}$.

The synchronization capability of the device relies essentially on the proximity of the physical parameters between the emitter and receiver. Thus, to expect perfect synchronization, we assume the same parameters for the master and slave, i.e., $\tau = \tau_s$, $\theta = \theta_s$, $\beta_1 = \beta_{1s}$, $\phi = \phi_s$, $I = I_s$. we introduce $\Delta T = T_s - T$ and using the values stated in Table 1 and 2 and taking $\phi = \pi/4$, we synchronize the emitter and receiver as it is shown in Fig.(2.9). When $\Delta T > 0$, the slave follows the master while it anticipates the master for $\Delta T < 0$. Hence, ΔT is the shift between the master and the slave. These results are in good agreement with those of experiment shown in Fig.(2.10). From these results it can be seen that the synchronization is independant of the coupling delay T_c. Thus, it does not depend on the flying time, time delays due to the electrical connections, and the response times of the system which play exactly the same role as the receivers delay time. The slight difference observed in experimental results is due to the fact that it is impossible to have the receiver perfectly identical to the emitter because of manufacturing errors which are unavoidable. Thus it is particularly important to explore the parameter mismatches.

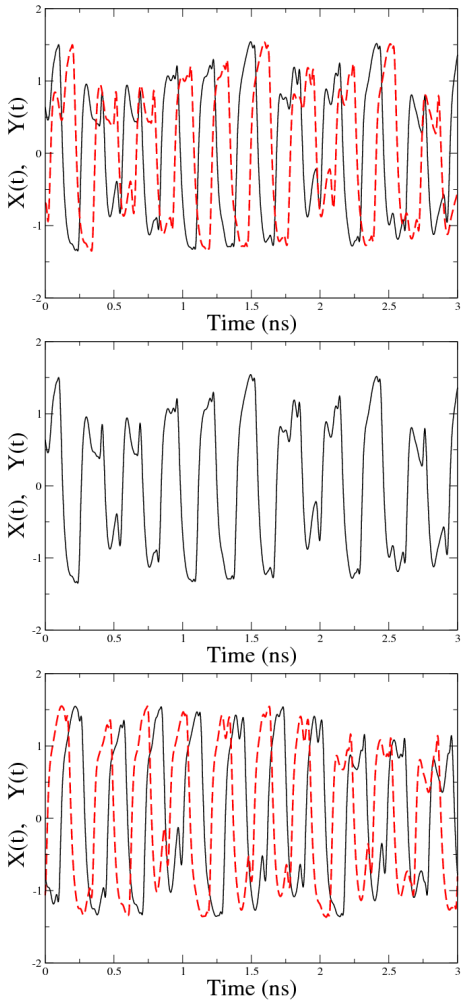

Figure 2.9: Emitter (solid line) and receiver (dashed line) time traces for $\Delta T = 0.1ns$ (top), $\Delta T = 0(center)$ and $\Delta T = -0.1ns$ (bottom). $J_0 = 1.5J_{th}$ and $\phi = \pi/4$

2.3.2 Single-parameter mismatch

The potential characterization of the effects of parameter mismatches can be done using two indicators:

- The maximum cross-correlation between the master and slave, defined as

$$MAX[\Gamma(s)] = MAX[\frac{\langle [x_p(t) - \langle x_p(t)\rangle][y_{p'}(t+s) - \langle y_{p'}(t)\rangle]\rangle}{\sqrt{[\langle x_p(t) - \langle x_p(t)\rangle\rangle]^2[\langle y_{p'}(t) - \langle y_{p'}(t)\rangle\rangle]^2}}] \qquad (2.19)$$

  which is the qualitative indicator showing how the trajectory is topologically distorted. When $\Delta T = 0$, $MAX[\Gamma(s)] = \Gamma(0)$.

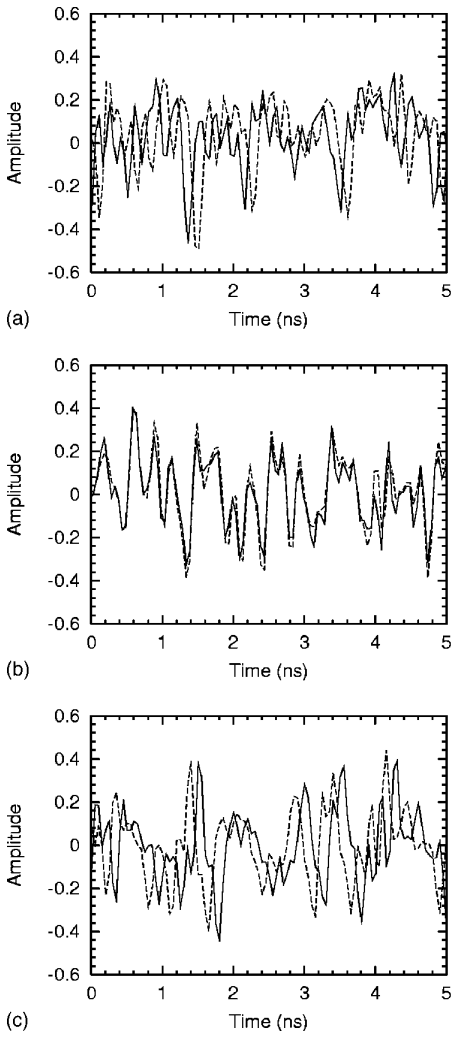

Figure 2.10: Experimental chaotic time traces, with x in continuous lines and y in dashed lines. The parameters are$P = 7.60\ mW$, $V_B = 1.05\ V$ (emitter), and $P_s = 3.91\ mW$,$V_{Bs} = 0.34\ V$ (receiver), $V_{\pi,DC} = 4.0\ V$, and a RF value (at 1 GHz) of $V_{\pi,RF} = 4.2\ V$ for $\lambda = 1550\ nm$, photodetector gain $2V/mW$ The amplification within within the nonlinear feedback loop was performed by a pair of RF amplifiers with a power gain of 18 dB and a bandwidth ranging from 30 kHz to 6.5 GHz(a)(top) $\Delta T = 0.15\ ns$, the slave is delayed relatively to the master; (b) (center) $\Delta T = 0.0$, the slave is isochronous to the master; (c) (bottom) $\Delta T = -0.15\ ns$, the slave anticipates the master [27]

- And a quantitative indicator measuring the time-averaged proximity between

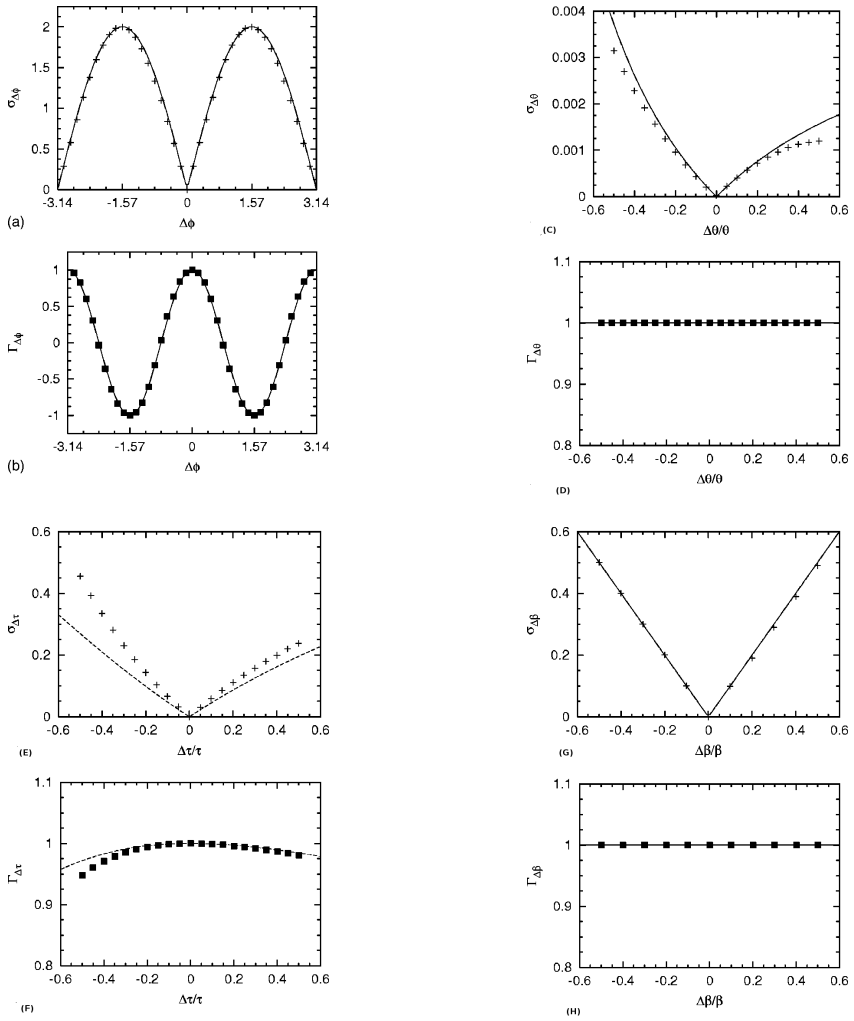

Figure 2.11: Average synchronization error ($\sigma_{\Delta\phi}$, $\sigma_{\Delta\tau}$, $\sigma_{\Delta\theta}$ and $\sigma_{\Delta\beta}$) and maximum correlation ($\Gamma_{\Delta\phi}$, $\Gamma_{\Delta\tau}$, $\Gamma_{\Delta\theta}$ and $\Gamma_{\Delta\beta}$) for the ϕ, τ, θ, β-mismatches, respectively. Analytical approximations are shown in solid line and numerical results in symbols. The parameters are: $\beta = 5$, $\tau = 50ps$, $\theta = 2\mu s$, $\phi = 0.1$, $T = 20ns$ [27]

the master and slave, namely the average synchronization error defined as

$$\sigma_{\Delta p} = \sqrt{\frac{\langle \varepsilon_{\Delta p}^2 \rangle}{\langle x_p^2 \rangle}} \tag{2.20}$$

where $\varepsilon_{\Delta p} = y_{p'}(t) - x_p(t)$ stands for the instantaneous synchronization, $\Delta p = p - p^{'}$ is the parameter mismatch and $x_p(t)$ and $y_{p'}(t)$ the time traces of the master and slave obtained with the parameter p and $p^{'}$ respectively. This last

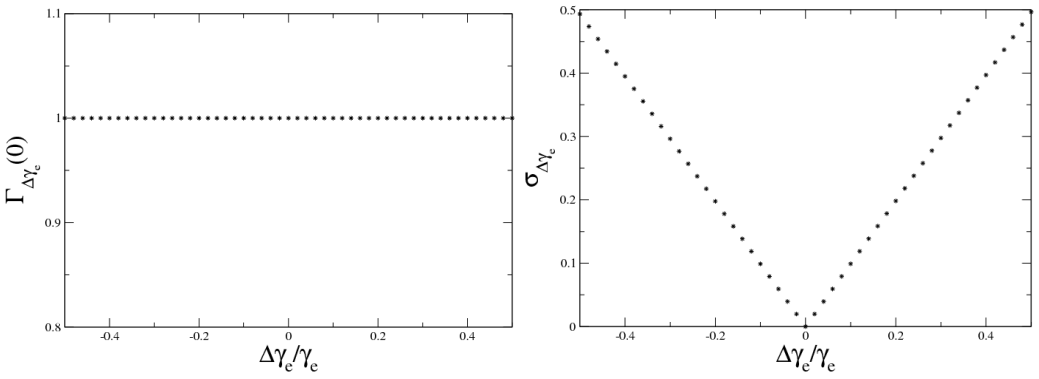

Figure 2.12: Maximum correlation (left) and average synchronization error (left for the γ_e-mismatch.

indicator is the sensibility one as well as an indicator of threshold of the minimum modulation index below that any encoded message cannot be recovered.

The single parameter mismatch is performed assuming all other mismatches to be zero. Fig.(2.11, a,b) shows that the synchronization error and cross-correlation at $\Delta\phi = \pm\pi/2$ are $\sigma_{\Delta\phi} = 2$ and $\Gamma_{\Delta\phi}(0) = -1$, respectively. It means exact anti-synchronization between the master and slave whereas for $\Delta\phi = 0$ we have $\sigma_{\Delta\phi} = 0$ and $\Gamma_{\Delta\phi}(0) = 1$ which mean perfect synchronization between the master and slave. From the results of parameter mismatches displayed in Fig.(2.11), it is seen that the most relevant mismatches are the offset phase where 0.005 rad induces 1% synchronization error, high cut frequency and nonlinear feedback-strengh where 1% mismatch originates almost 1% and 0.5% synchronization error, respectively. In practice, however, the parameter mismatch occurs for several parameters at the same time. Nevertheless, choosing appropriate parameters and the mismatches can be compensated enough to obtain satisfactory synchronization. One can notice that the mismatch of the feedback-strengh is a global mismatch effect introduced by the SC laser, the amplified gain and the photodiode sensibility. Fig.(2.12) shows inverse carrier lifetime mismatch as a function of SC laser mismatch plotted for our parameters. One can see that this single parameter mismatch of the laser is similar to the overall laser mismatch (β). It is seen perfect correlation at equal time independently to the γ_e-mismatch while the synchronization error linearly increases with respect to $\Delta\gamma_e$. It is due to the fact that, despite the good synchronization, this parameter affects considerably the amplitude of the signal. Therefore, the master and slave synchronize at different amplitude depending on the mismatch. To the best of our knowledge, all the laser parameter mismatches play the same role as $\Delta\gamma_e$. When the synchronization conditions are satisfied, the message is encoded within the chaotic carrier

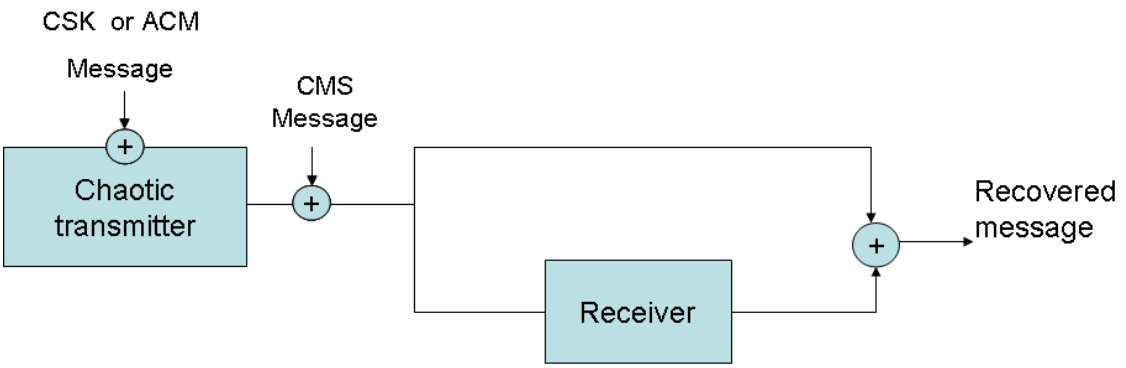

Figure 2.13: skeleton of chaotic masking message

2.3.3 Encoded/Decoded message

Masking communications based on chaotic dynamics can be useful only if we are able to recover the message. The encoded message should remain hidden from the eavesdroppers without loosing its original quality. Basically, the chaos encryption is based on the standard principle that we schematically present in Fig.(2.13). In this framework, the message is embedded within the chaotic carrier provided by the emitter. Then, the signal is split and one part is sent to the receiver before being sent to the combiner together with the second part. First of all, the message to be encrypted should be smaller compared to the amplitude of chaos to ensure the secrecy as well as to avoid large distortions of the transmitter output which could prevent the receiver from synchronization.

There are several ways to encode the message. The most important ones include:

♣ Chaos shift key (CSK): In this type of the scheme, the digital message directly modulates the current to the transmitter laser. Thus, the current to the transmitter laser switches between two distinct levels depending on whether a "0" or "1" bit is transmitted. Meanwhile, the receiver laser is biased at a fixed current level which is the level at which "0"bit is transmitted. In the transmitter laser, the message is recovered by measuring the synchronization error between the transmitter and receiver.

♣ Chaos masking (CMS): In this case, the message is added on the chaotic waveform after the chaotic waveform leaves the optoelectronic feedback loop of the transmitter. Thus, the message does not affect the feedback loop of the transmitter.

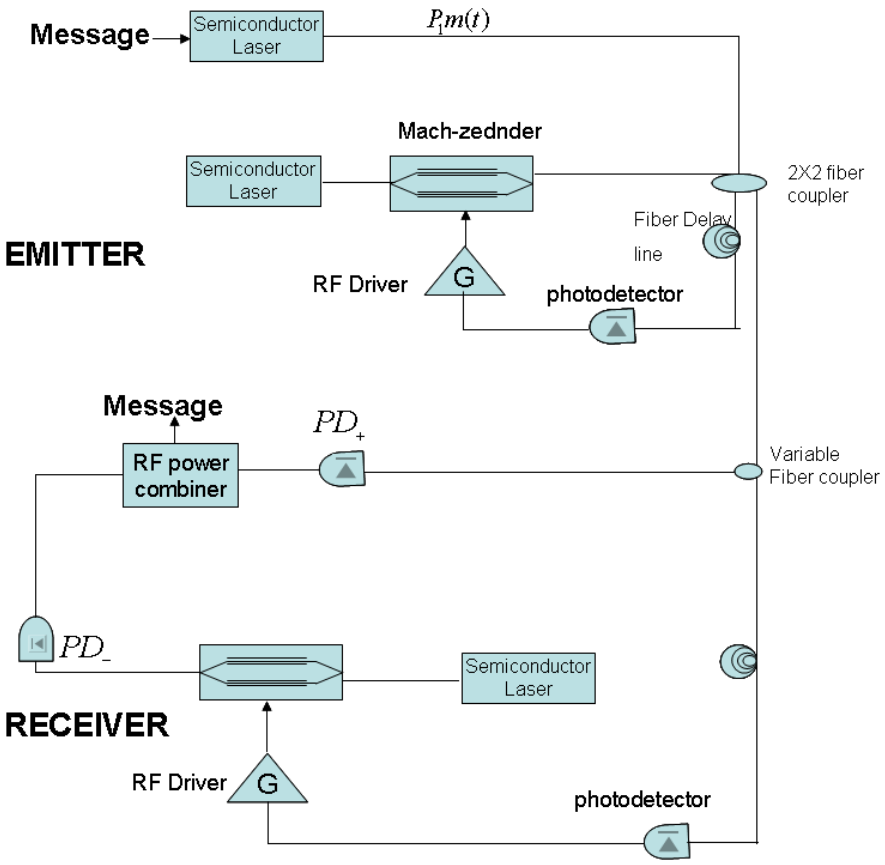

Figure 2.14: encryption/decryption setup

In this type of the scheme, the two electro-optical devices (emitter and receiver) are always biased at the same current level when they synchronize perfectly. At the combiner, the message is performed by subtracting the receiver output and the second part of the signal which is the emitter output and message.

♣ Chaos modulation: possible encoding and decoding schemes include additive chaos modulation (ACM) and multiplicative chaos modulation (MCM). The widespread one is ACM scheme where the message is added on the chaotic waveform within the optoelectronic feedback loop of the transmitter. Therefore, the dynamics of the transmitter laser is also affected by the encoded message. At the receiver, message is achieved through the same process as that in the CMS scheme.

When the message is encoded, its effects can affect the system performances (dynamics, synchronization and communication performance) depending on encod-

ing/decoding scheme. The first experimental demonstration of the effects of message encoding and decoding on the chaotic dynamics, chaos synchronization, and chaotic communication performance of a chaotic optical communication system has been reported in [37]. Numerical simulations have shown that the ACM scheme can increase the complexity of the chaotic waveforms while at the same time it can maintain the synchronization quality before and after a message is encoded [38].

In the following, we encode the message by ACM scheme. We assume the message to be encoded and decoded in the chaotic system as a sequence of a non-return-to- zero (NRZ) pseudorandom digital bits at $1.0Gbit/s$ bit rate. A NRZ line code is a binary code in which "1s" are represented by one significant condition (usually a positive voltage) and "0s" are represented by some other significant condition (usually a negative voltage), with no other neutral or rest condition. We add the message using another semiconductor laser with wavelength close to that of the emitter which is modulated by the digital message to be sent in the chaotic carrier. The complete schematic setup with encoded/decoded mechanism is shown in Fig.(2.14). The output of this laser diode containing message is $p_1 m(t)$ where $m(t)$ takes 1 bit when an optical power p_1 is transmitted and 0 bit when no optical power is transmitted. The mixing is performed through an all-optical mean namely 2X2 fiber coupler. When the message is embedded within the chaos, eq.(2.13) for the emitter becomes

$(1+\frac{f_L}{f_H})V(t)+\frac{1}{2\pi f_L}\frac{dV(t)}{dt}+2\pi f_H \int_{t_0}^{t} V(t)ds = gGsk_1 Icos^2(\frac{\pi}{2}\frac{V(t-T)}{V_{\pi RF}} + \frac{\pi}{2}\frac{V_B}{V_{\pi DC}}) + P_1 m(t)$

which normalization leads to

$$x + \tau\frac{dx}{dt} + \frac{1}{\theta}w = \beta_1 I\cos^2[x(t-T)+\phi] + \alpha m(t) \tag{2.21}$$

$p_1 m(t)$ is a binary message light beam and α is the P_1-normalized value, i.e., $\alpha = \pi P_1/2V_\pi$ with $\alpha << (\beta_1 I)$. Thus, the transmitted signal from the emitter is $s_T = \beta_1 I\cos^2[x(t-T)+\phi] + \alpha m(t)$. Subsequently, this signal is split into two parts by a variable fiber coupler and one part travels through the receiver feedback loop while a second part serves to decode the encoded message. Similarly to the previous study, we find that the receiver driven by the emitter with the embedded message is ruled by (assuming the same parameters for the emitter and receiver)

$$y + \tau\frac{dy}{dt} + \frac{1}{\theta}w_s = \beta_1 I_s\cos^2[x(t-T)+\phi] + \alpha m(t-T) \tag{2.22}$$

On the other hand, the output of the receiver Mach-Zehnder crossing the PD_- photodiode is expressed by $K\beta_1 I_s\cos^2[y(t)+\phi_s]$ where k is a factor referring to the

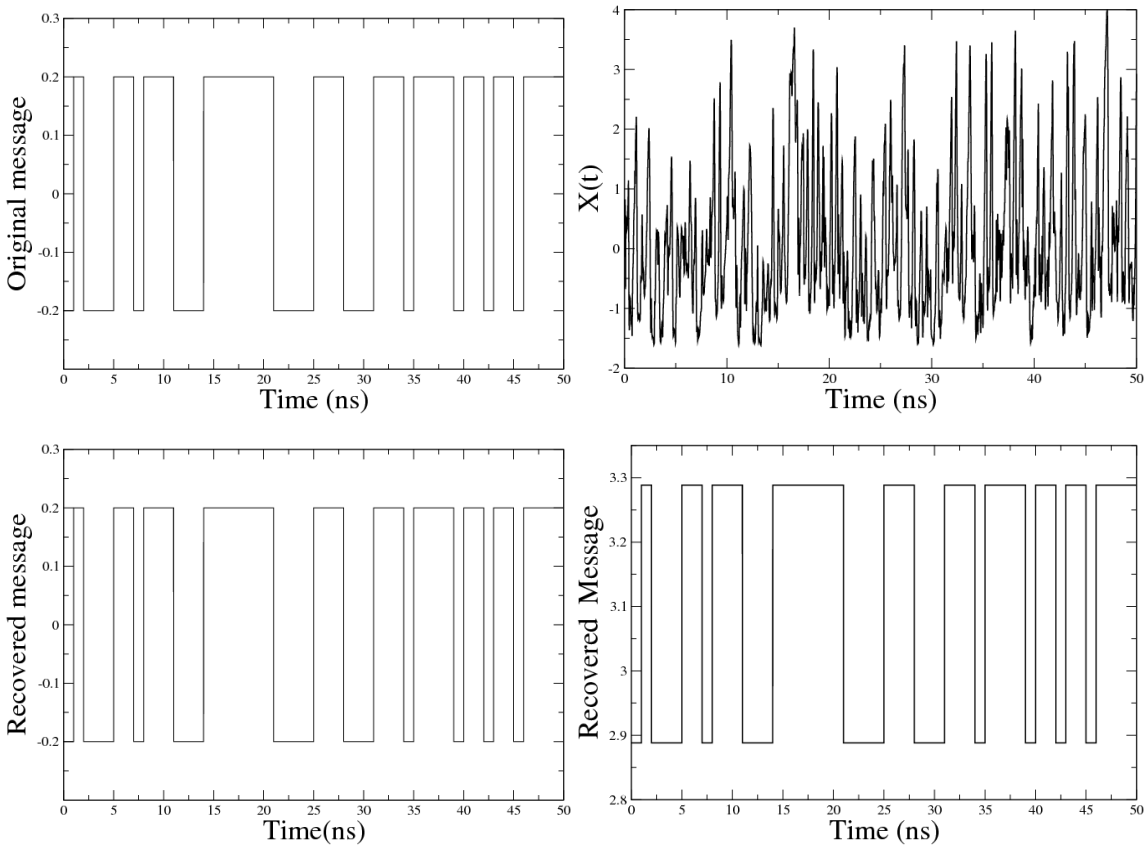

Figure 2.15: original message (top and left), emitter time trace with message (top and right), recovered message (bottom-left) by substraction and recovered message (bottom-left) by tuning the receiver off-set phase for $J_0 = 1.5J_{th}$, $J_1 = 0.1J_0$ and $\phi = \pi/4$

PD_- sensitivity and fiber coupler used. Subsequently, this electrical signal is sent in the combiner together with the second part which after crossing PD_+ photodiode becomes $K^{'}(\beta_1 I \cos^2[x(t)+\phi] + \alpha m(t))$ where $k^{'}$ refers to PD_+ sensitivity and fiber coupler. There are two ways to recover the message with the combiner:

- The first one is to cancel the chaos by tuning the receiver offset phase ϕ_s. It takes the advantage of the perfect anti-synchronization when the phase difference $\Delta\phi = \pm\pi/2$. Thus during the recombination at the combiner output, the time traces of the master and slave which perfectly synchronize in opposition cancel out each other. The output of the combiner is given by

$$S_c(t) = K^{'}(\beta_1 I \cos^2[x(t)+\phi] + \alpha m(t)) + K\beta_1 I_s \cos^2[y(t)+\phi_s] \qquad (2.23)$$

If the receiver and the emitter synchronize perfectly, $x(t) = y(t)$ and $I(t) =$

$I_s(t)$. In addition, taking $k = k^{'}$ and $\phi_s = \phi + \pi/2$, we have from eq.(2.23)

$$S_c(t) = k\beta_1 I + K\alpha m(t). \tag{2.24}$$

which is the message shifted by $k\beta_1 I$. It is possible to cancel this shift using the bandpass filtering of usual high speed preamplified photodiodes [28].

- The second way to recover the hidden message is to subtract off the second part of the signal and the output of the receiver PD_+.

  $$S_c(t) = K^{'}(\beta_1 I \cos^2[x(t) + \phi] + \alpha m(t)) - K\beta_1 I_s \cos^2[y(t) + \phi_s] \tag{2.25}$$

  With the same parameters, perfect synchronization means $x(t) = y(t)$ and $I(t) = I_s(t)$ and taking $k = k^{'}$ and $\phi_s = \phi$, we have from eq.(2.25)

  $S_c(t) = K\alpha m(t)$,

  which gives the recovered message.

  For $K = 1$ and $\alpha = 0.2$, the recovered message is shown in Fig.(2.15) collected with both methods..

We have shown in this chapter that it is possible to induce chaos from SC laser by introducing nonlinear electro-optical loop. We have shown how the chaos generation can help to secure the message. But, strictly speaking, even though J_0 is tuned to induce chaos in the system, it does not guarantee strong chaos required for encryption for most of the phases when $J_0 \leq 1.8J_{th}$. Present-day devices use $5 \leq \beta \leq 10$ which corresponds in our case to $1.81J_{th} \leq J_0 \leq 2.63J_{th}$. Our purpose is to induce more complexity of chaotic carrier even with J_0 smaller than $1.5J_{th}$.

Chapter 3

Semiconductor lasers with double feedback Loop

In this chapter, we explore the previous electro-optical device in which a fraction of the signal performed at the oscillator feedback loop is injected back in the active layer of the laser. This process generates an unidirectional coupling from the filtering loop to the inversion population density. We will explore the situation in two distinct schemes. First, we will devote to the scheme in which the feedback pump current is linear. In the second scheme, we deal with nonlinear feedback pump current. In both cases, we briefly describe the model, as well as, its properties upon the synchronization, parameter mismatches and encoded/decoded message in comparison with the results described in chapter 2.

3.1 Electro-optical device subjected to Linear feedback pump current

3.1.1 The Model

We study the setup shown in Fig. (**??**). In the optoelectronic feedback loop, the optical output signal of the Mach-Zehnder crosses the delay line, then it is converted into electronic signal by the photodetector and fed into the RF driver. After its amplification, the electronic signal is split into two parts. One part is applied directly to the Mach-Zehnder while the second part is re-injected back in the active layer of the laser which serves as the light source. Therefore the light source feeding the Mach-Zehnder switches from the continuous wave form to the regime depending on that of the RF voltage. Thus, in the chaotic regime for instance, the light source erratically fluctuates. Taking an analog to the previous model, the global dynamics of the system is governed by the set of eq.(3.1), where the parameters are written in Table 1 and 2.

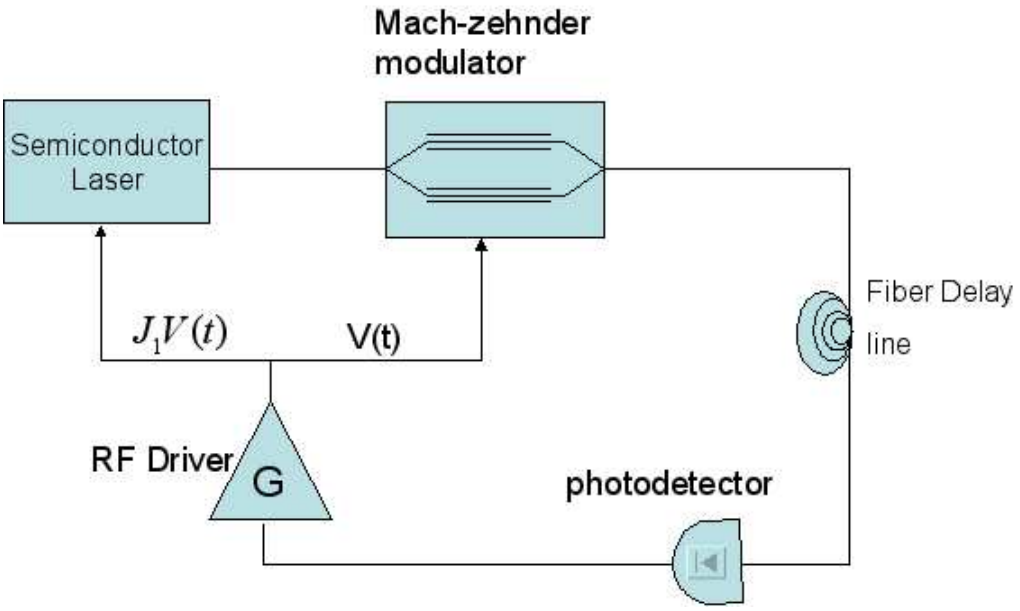

Figure 3.1: setup of semiconductor laser with two electro-opticalfeedback

$$\begin{cases} \frac{dI}{dt} = (G-\gamma)I \\ \frac{dN}{dt} = J_0 - \gamma_e N - GI + J_1 X(t) \\ x + \tau\frac{dx}{dt} + \frac{1}{\theta}w = \beta_1 I\cos^2[x(t-T)+\phi] \\ \frac{dw}{dt} = x \end{cases} \quad (3.1)$$

we notice an extra term on the inversion population density equation coming from the feedback pump current. In this equation, J_1 stands for the feedback constant of the pump current. Because the carrier number N depends to the RF voltage, the overall normalized gain β becomes an implicit function of x(t) and therefore of time ($\beta = \beta_1 I \neq Constant$).

3.1.2 Theoretical and numerical study

The system under study has the same single stationary point as previously investigated namely, (x_s, w_s, I_s, N_s) where
$x_s = 0, w_s = \theta\beta_1 I_s\cos^2\phi$,
$I_{st} = \frac{J_0 g_m - \gamma_e g_m N_0 - \gamma_e\gamma}{\gamma(g_m + s\gamma_e)}, N_{st} = \frac{g_m N_0 + \gamma + sJ_0}{g_m + s\gamma_e}$.
The stability of this fixed point is found assuming $x = x_s + x_1$, $w = w_s + w_1$, $I = I_s + I_1$ and $N = N_s + N_1$, and taking an analog to previous section , we obtain

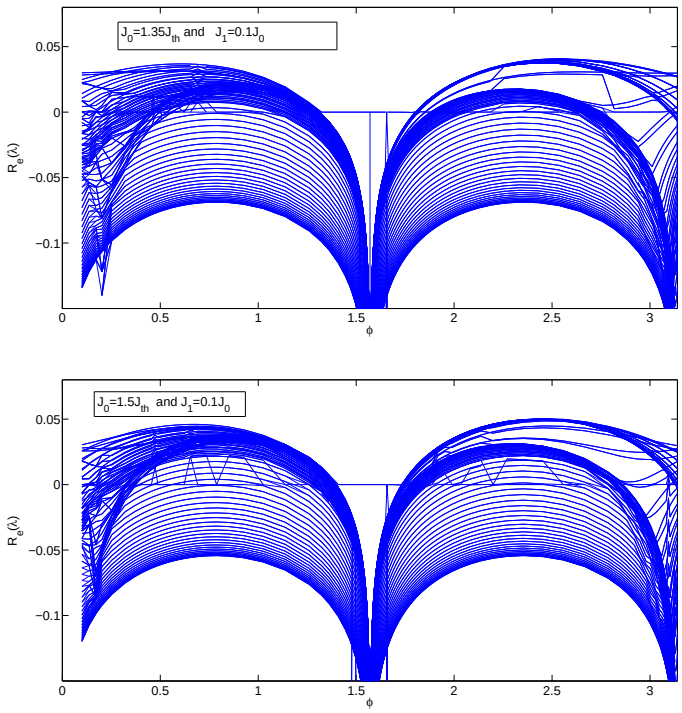

Figure 3.2: Real part of solutions given by the eigen equation versus off-set phase for $J_1 = 0.1J_0$

a set of equations

$$\begin{cases} \frac{dx_1}{dt} = -\frac{1}{\tau}x_1 - \frac{1}{\tau\theta}w_1 + \frac{\beta_1 \cos^2\phi}{\tau}I_1 - \frac{\beta_1 I_{st}}{\tau}sin(2\phi)x_1(t-T) \\ \frac{dw_1}{dt} = x_1 \\ \frac{dI_1}{dt} = -\frac{s\gamma I_{st}}{1+sI_{st}}I_1 + \frac{g_m I_{st}}{1+sI_{st}}N_1 \\ \frac{dN_1}{dt} = J_1 x_1 - (\gamma + \frac{s\gamma I_{st}}{1+sI_{st}})I_1 - (\gamma_e + \frac{g_m I_{st}}{1+sI_{st}})N_1 \end{cases} \tag{3.2}$$

Once more assuming $x_1 \sim e^{\lambda t}$, $w_1 \sim e^{\lambda t}$, $I_1 \sim e^{\lambda t}$ and $N_1 \sim e^{\lambda t}$, the set of eq.(3.2) can be written as a 4 by 4 matrix with eigen equation given by the determinant

$$\text{detM}= \begin{vmatrix} -\lambda - \frac{1}{\tau} - \frac{\beta_1 I_{st}}{\tau}sin(2\phi)e^{-\lambda T} & -\frac{1}{\tau\theta} & \frac{\beta_1 \cos^2\phi}{\tau} & 0 \\ 1 & -\lambda & 0 & 0 \\ 0 & 0 & -\lambda - \frac{s\gamma I_{st}}{1+sI_{st}} & \frac{g_m I_{st}}{1+sI_{st}} \\ J_1 & 0 & -\gamma + \frac{s\gamma I_{st}}{1+sI_{st}} & -\lambda - \gamma_e - \frac{g_m I_{st}}{1+sI_{st}} \end{vmatrix} =0$$

where λ is the eigenvalue. From this determinant, we have

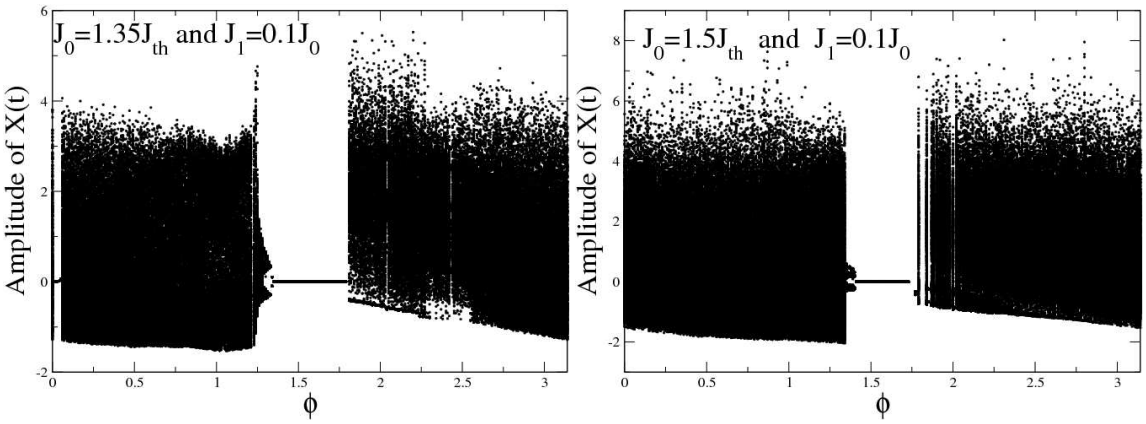

Figure 3.3: Bifurcation diagram versus off-set phase ϕ
for different injection current J_0

$$\lambda^4 - \lambda^3[a_{44} + a_{33} + \tilde{a}_{11} + a_{11}e^{-\lambda T}] + \lambda^2[a_{33}a_{44} - a_{43}a_{34} + \tilde{a}_{11}(a_{44} + a_{33}) + a_{11}(a_{44} + a_{33})e^{-\lambda T} - a_{12}] + \lambda[(a_{43}a_{34} - a_{33}a_{44})\tilde{a}_{11} + (a_{43}a_{34} - a_{33}a_{44})a_{11}e^{-\lambda T} + a_{33}a_{12} + a_{12}a_{44} - a_{41}a_{13}a_{34}] - a_{12}a_{44}a_{33} + a_{12}a_{43}a_{34} = 0 \tag{3.3}$$

where
$a_{11} = -\frac{\beta_1 I_{st}}{\tau} sin(2\phi)$; $\tilde{a}_{11} = -\frac{1}{\tau}$; $a_{12} = -\frac{1}{\tau\theta}$
$a_{13} = \frac{\beta_1 \cos^2\phi}{\tau}$; $a_{33} = -\frac{s\gamma I_{st}}{1+sI_{st}}$; $a_{34} = \frac{g_m I_{st}}{1+sI_{st}}$
$a_{41} = J_1$; $a_{43} = -\gamma + \frac{s\gamma I_{st}}{1+sI_{st}}$; $a_{44} = -\gamma_e - \frac{g_m I_{st}}{1+sI_{st}}$

The computation of this eigen equation allows to qualify the effects of J_1 on the steady state by comparison with that without the feedback current. Therefore, Using DDE-BIFTOOL algorithm in Matlab, we collect the results displayed in Fig.(3.2) with $J_1 = 0.1J_0$. We can notice from Fig.(3.2) that, in both cases, only the steady states close to $\pi/2$ remain with almost the same width while others have disappeared.

Next, we estimate the effects of J_1 on the unstable area by plotting the bifurcation diagram with respect to ϕ. The steady states shown in Fig.(3.3) are in good agreement with those found by the stability analysis. Compared to the previous case ($J_1 = 0.0$), the steady states near to 0 and π offset phase and periodic areas become chaotic.

On the contrary of the previous case, Fig.(3.4) shows chaotic behaviour from $J_0 = 1.3J_{th}$ corresponding to $\beta = 1.8$. It is therefore seen that with J_1 the value of J_0

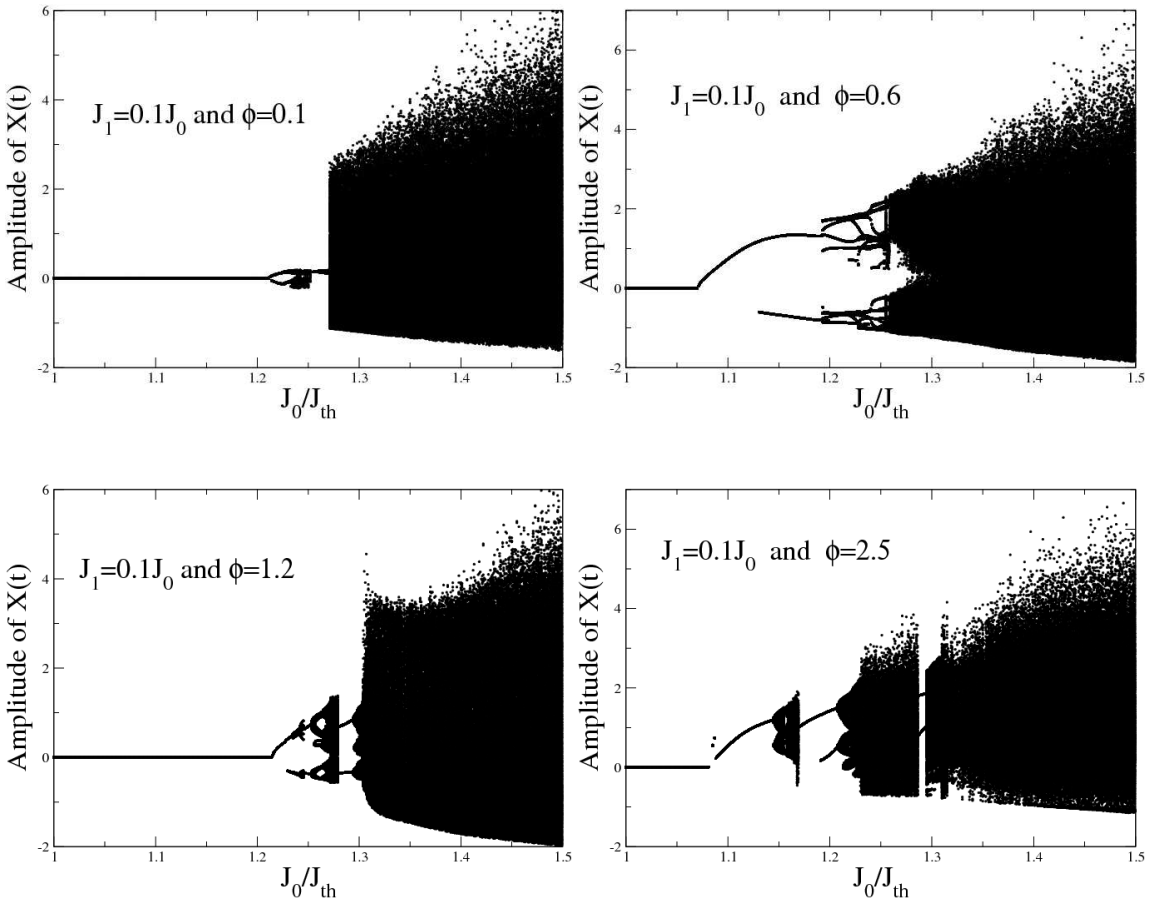

Figure 3.4: Bifurcation diagram versus injection current J_0 for different off-set phase ϕ

required to induce chaotic behaviour can be lowered from $J_0 = 1.6J_{th}$ to $J_0 = 1.3J_{th}$. When J_0 is enough, the system moves directly from steady state to chaos for some values of phase (particularly the small ones like $\phi = 0.1$) and passes through the bifurcation otherwise. We also notice large fluctuations of the signal when J_1 increases. However, the presence of the low cutoff integral term in eq. (2.12) imposes the mean value of X(t) to be zero in order to ensure the convergence of the solution even at infinite. As a consequence, the average of the total normalized gain $\langle\beta\rangle = \beta_1\langle I\rangle$ remains unchanged. For example with our parameters, $\langle\beta\rangle = 3.08$ when $J_1 = 0$ and $\langle\beta\rangle = 3.10$ for $J_1 = 0.1J_0$.

Another potential approach to qualify this chaos can be done using the nor-

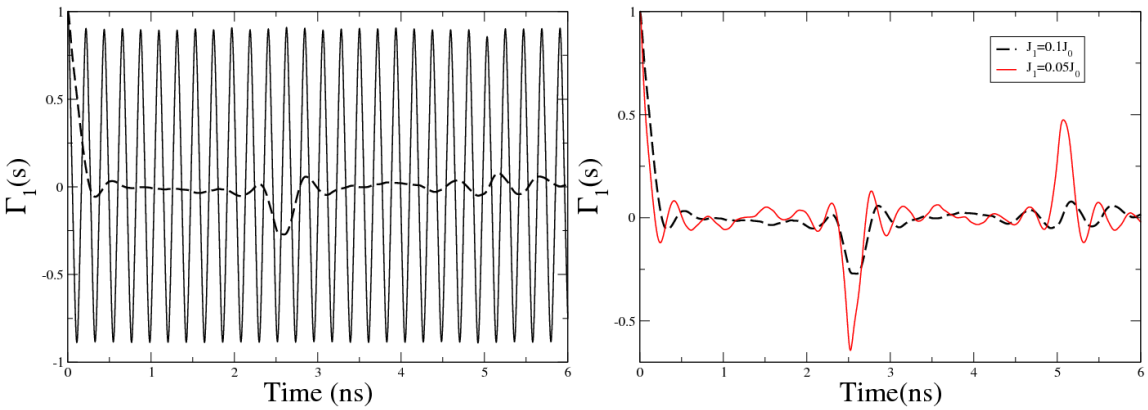

Figure 3.5: Auto-correlation function with respect to the time for $J_1 = 0.0$ (left-solid line), $J_1 = 0.1$ (left-dashed line), $J_1 = 0.05$ (right-solid line),$J_1 = 0.1$ (right-dashed line)

malized auto-correlation function defined as

$$\Gamma_1(s) = \frac{\langle [x(t) - \langle x(t)\rangle][x(t+s) - \langle x(t)\rangle]\rangle}{[\langle x(t) - \langle x(t)\rangle\rangle]^2}, \tag{3.4}$$

which is the qualitative indicator showing how the points upon the trajectory are correlated in time. From Fig.(3.5), it is seen that the correlation function decreases faster when J_1 is added. it means the feedback pump current increases the unpredictability dynamics of the chaotic carrier. The points of the trajectory separated by the delay time T keep some correlation, but this correlation damages when the complexity of the chaos increases or when the time separation is large enough. This is known as one of the characteristics of differential with constant delay systems. Thus, the application of the feedback pump current allows to increase the complexity of the chaos complexity. In order to make it profitable, we synchronize in next section a pair of this device.

3.1.3 Synchronization of two electro-optical devices subjected to feedback pump current

We consider two separate electro-optical systems with similar architecture as it is shown in Fig.(3.6). The receiver is still fed only by the signal coming from the emitter and its feedback pump current is taken at its RF driver output. The dynamics of the system is now described by

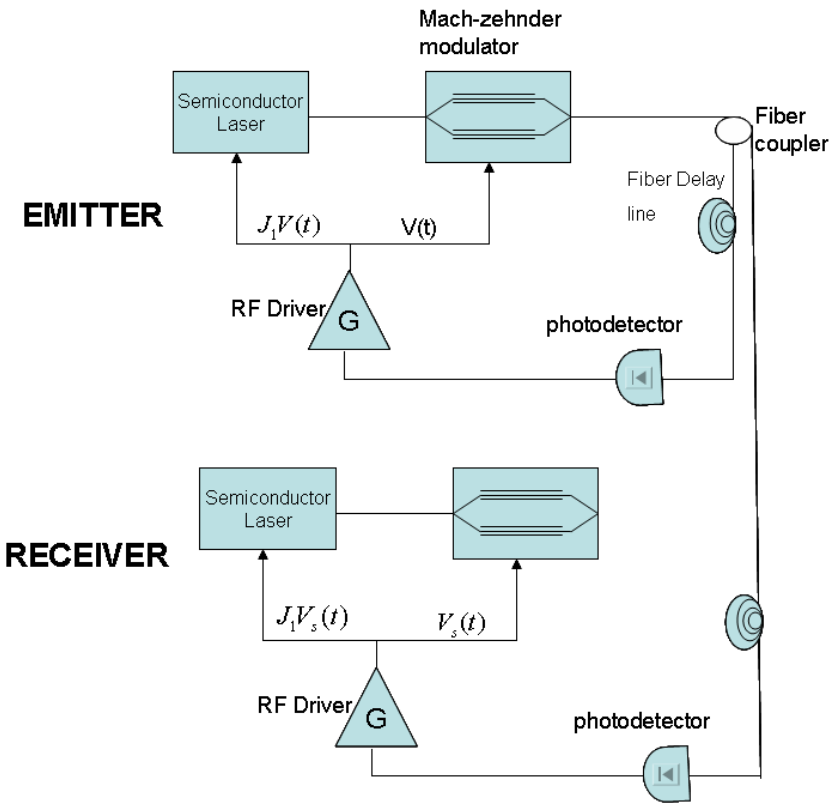

Figure 3.6: setup of semiconductor laser with two electro-opticalfeedback

$$Emitter: \begin{cases} \frac{dI}{dt} = (G-\gamma)I \\ \frac{dN}{dt} = J_0 - \gamma_e N - GI + J_1 X(t) \\ x + \tau\frac{dx}{dt} + \frac{1}{\theta}w = \beta_1 I\cos^2[x(t-T)+\phi] \\ \frac{dw}{dt} = x \end{cases} \tag{3.5}$$

$$receiver: \begin{cases} \frac{dI_s}{dt} = (G_s-\gamma_s)I_s \\ \frac{dN_s}{dt} = J_0 s - \gamma_e s N_s - G_s I_s + J_{1s} y(t) \\ y + \tau_s\frac{dy}{dt} + \frac{1}{\theta_s}w_s = \beta_{1s} I_s\cos^2[x(t-T_s)+\phi_s] \\ \frac{dw_s}{dt} = y \end{cases} \tag{3.6}$$

where the subscript "s" denotes the slave and $y(t) = \frac{\pi V_s(t)}{2V_\pi}$. As we emphasized earlier, the master and slave should be closer as possible to synchronize perfectly. Thus we assume both to be identical, i.e., the same parameters for both devices:

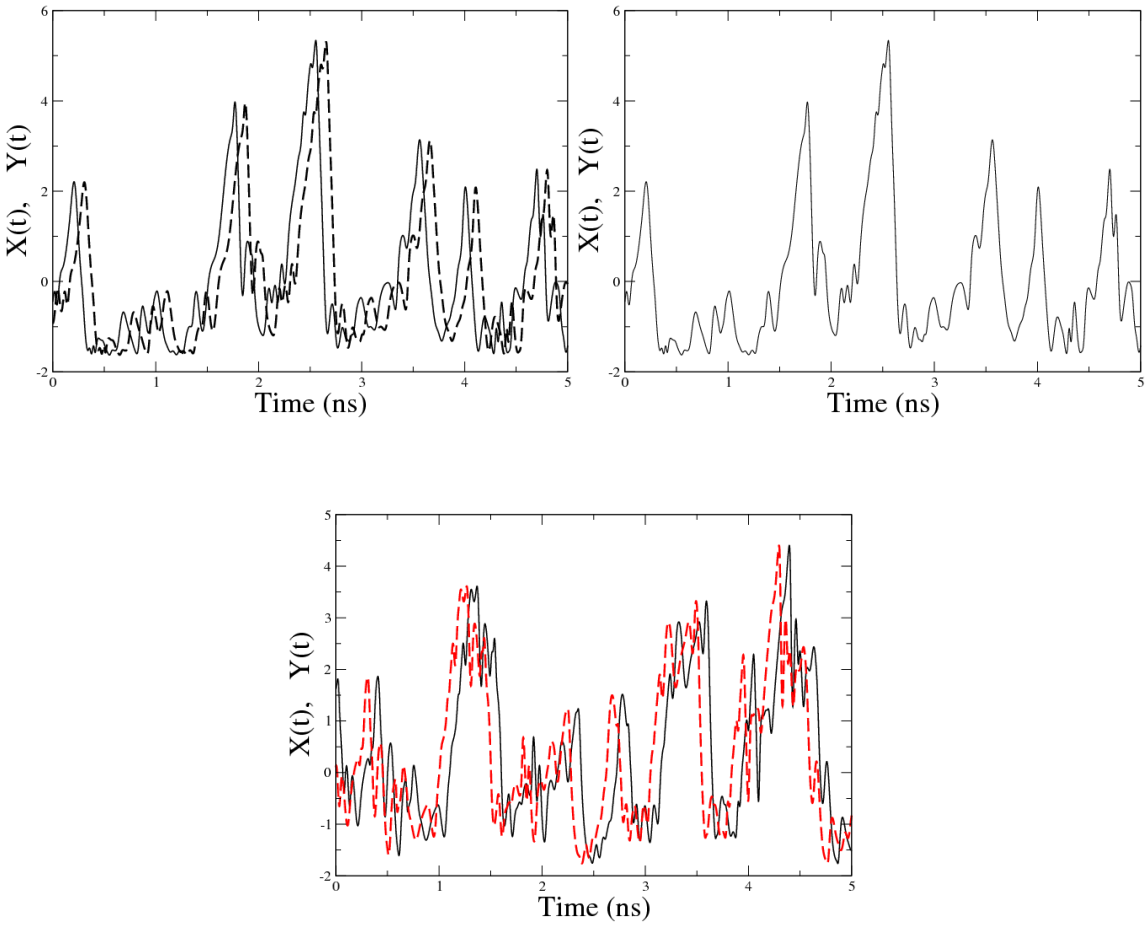

Figure 3.7: Emitter (solid line) and receiver (dashed line) time traces for $\Delta T = 0.1ns$ (top-left), $\Delta T = 0$ (top-right) and $\Delta T = -0.1ns$ (bottom). $J_0 = 1.5J_{th}$,$J_1 = 0.1J_0$ and $\phi = \pi/4$

$\gamma = \gamma_s$, $g_m = g_{ms}$, $N_0 = N_{0s}$, $s = s_s$, $J_0 = J_{os}$, $\gamma_e = \gamma_{es}$, $J_1 = J_{1s}$ for the laser parameters and

$\tau = \tau_s$, $\theta = \theta_s$, $\beta_1 = \beta_{1s}$, $\phi = \phi_s$ for the feedback loop.

We plot in Fig.(3.7) the time traces for different values ΔT. In agreement with synchronization principles shown the previous chapter, the slave follows the mater when $\Delta T > 0$, anticipates the master when $\Delta T < 0$ or similar when $\Delta T = 0$. These results show that the extra-feedback added does not matter for the synchronization when devices are identical. But it could seriously impede the synchronization quality when the mismatch is taken into account since in practice, it is impossible to build a pair of identical devices. Therefore, more attention should accordingly devote to parameter mismatch.

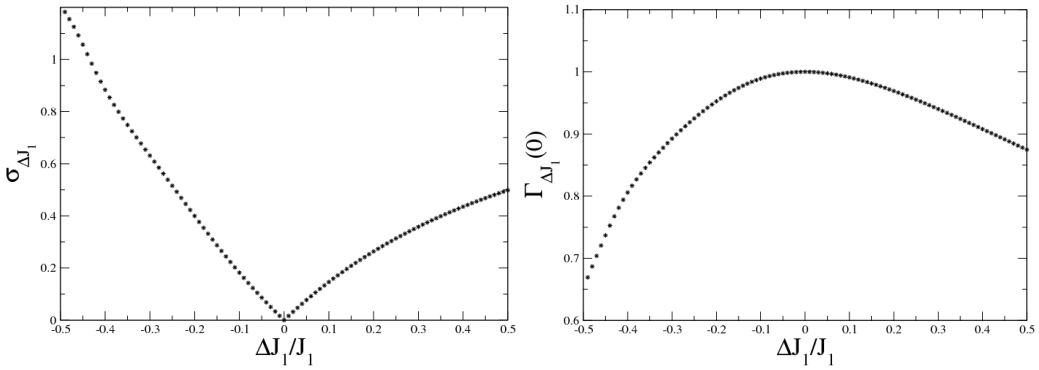

Figure 3.8: Average synchronization error (right) and maximum correlation (left) for J_1 mismatch at equal time

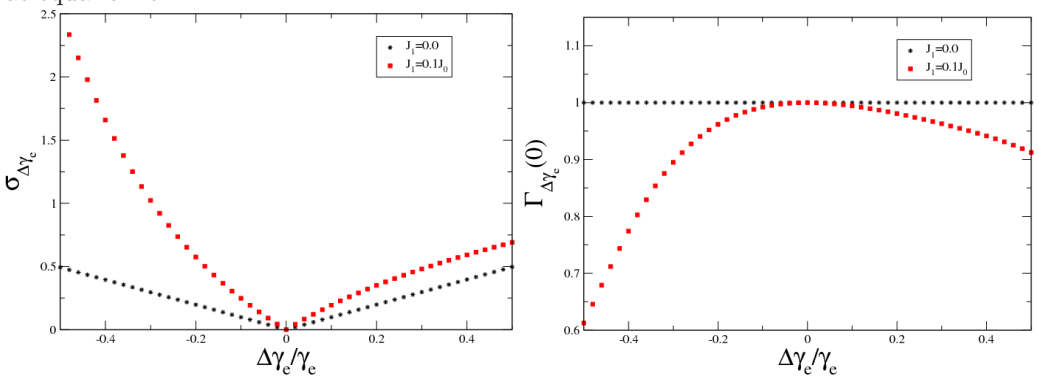

Figure 3.9: Average synchronization error (right) and maximum correlation (left) for γ_e mismatch at equal time

3.1.4 Single-parameter mismatch

***Pump current parameter mismatch** J_1

The mismatch in feedback pump current coefficient can stem to the fiber used to split the signal. Assuming that others parameters are equal for the master and the slave, we display in Fig.(3.8) the synchronization error and the maximum cross-correlation. The synchronization is relatively more sensitive to the mismatch in feedback pumped current parameter since 1% mismatch induces almost 1% of synchronization error. This ratio is not enough to damage badly the synchronization quality. However, it is damaged seriously when the feedback current parameter of the slave is greater than the master one in relative shift greater than 10%.

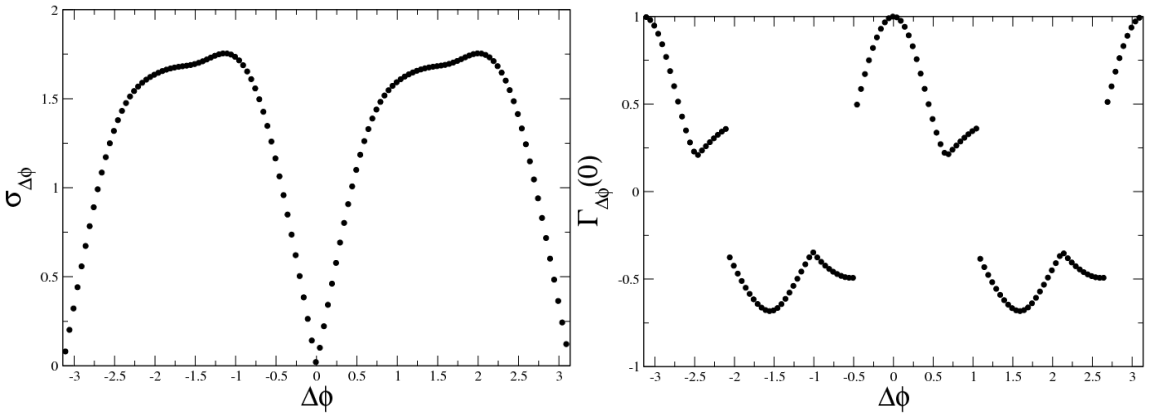

Figure 3.10: Average synchronization error (right) and maximum correlation (left) for ϕ mismatch at equal time

***Inverse carrier lifetime mismatch γ_e**

It can stem in slight difference in average of the recombined time. It can be due to spontaneous emission, etc.. It is found from Fig.(3.9) that the synchronization is more sensitive to the γ_e mismatch in presence of J_1. Comparing the two results obtained with $J_1 = 0.0$ and $J_1 = 0.1J_1$, respectively, we notice that the presence of J_1 imposes the two lasers to be similar enough to give satisfying synchronization since 1% error induces 2% synchronization error. On the contrary of the previous case ($J_1 = 0.0$), it considerably affects the synchronization quality when the mismatch is greater than 1%.

***off-set phase mismatch ϕ**

This parameter mismatch is performed on the bias electrode half-wave $V_{\pi RF}$ or DC component V_B assuming others parameters of the system equal. From the results displays in Fig.(3.10), the perfect synchronization occurs at null-mismatch with π-period. However, the $\phi - mismatch$ shows the exact anti-synchronization is not satisfied as we showed in section 2.3.2 since $\Gamma_{\Delta\phi}(0) = -1$ or $\sigma_{\Delta\phi} = 2$ is by far being satisfying.

3.1.5 Encoded/Decoded message

The architecture of decryption is also similar to that described in Fig.(2.14) using ACM scheme. Similarly to the previous study, we find that the emitter and receiver

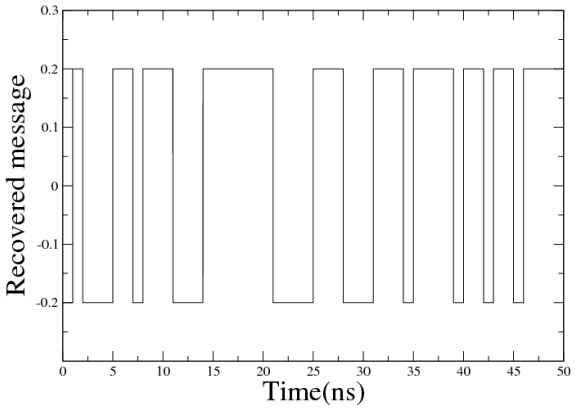

Figure 3.11: recovered message for $J_0 = 1.5J_{th}$, $J_1 = 0.1J_0$ and $\phi = \pi/4$

with the embedded message are ruled by (assuming the same parameters for the emitter and receiver)

$$x + \tau\frac{ds}{dt} + \frac{1}{\theta}w = \beta_1 I\cos^2[x(t-T)+\phi] + \alpha m(t-T) \tag{3.7}$$

$$y + \tau\frac{dy}{dt} + \frac{1}{\theta}w_s = \beta_1 I_s\cos^2[x(t-T)+\phi] + \alpha m(t-T) \tag{3.8}$$

where I and I_s are varying in time. Because of that, eq.(2.24) does not give the message shifted as previously investigated since in this regime I is proportional to I. moreover, in regard to offset phase mismatch, it is impossible to have the perfect anti-synchronization by tuning the off-set phase. As a consequence, the only way to decode the message is by subtraction. Thus in the conditions described in section 2.3.3, the output of the combiner is given by

$$S_c(t) = K^{'}(\beta_1 I\cos^2[x(t)+\phi] + \alpha m(t)) - K\beta_1 I_s\cos^2[y(t)+\phi_s] \tag{3.9}$$

When both devices synchronize perfectly, we have $x(t) = y(t)$ and $I(t) = I_s(t)$ and taking $k = k^{'}$ and $\phi_s = \phi$, the analytical solution is given by

$S_c(t) = K\alpha m(t)$, For $K = 1$ and $\alpha = 0.2$, the results obtained from eq.(3.9) are collected in Fig.(3.11).

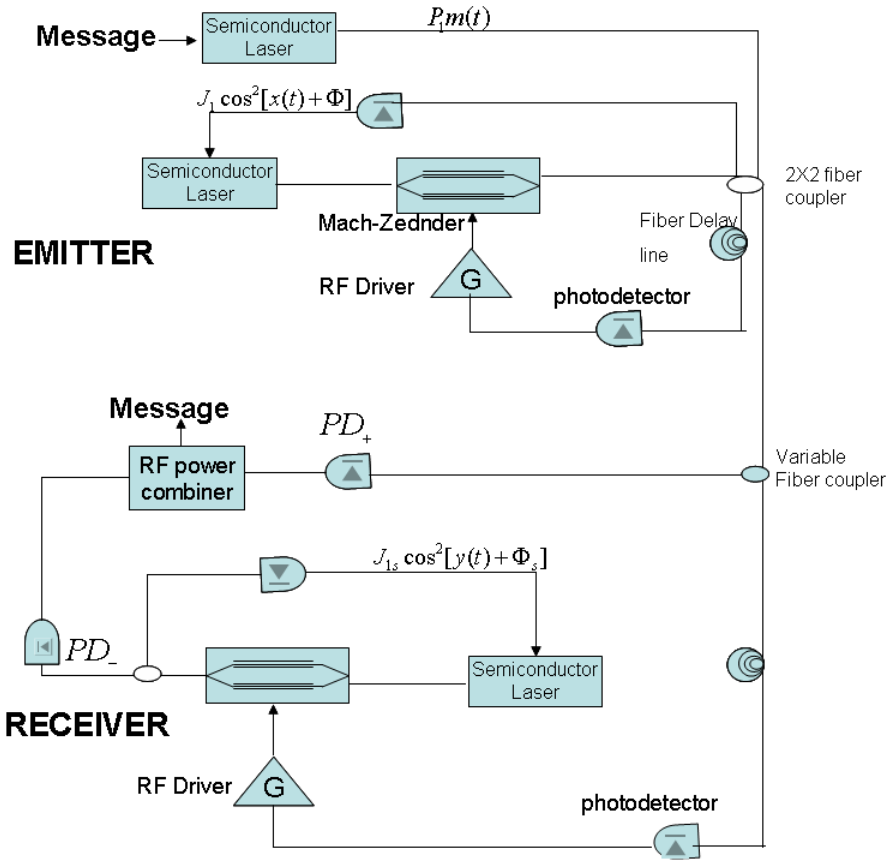

Figure 3.12: setup of semiconductor laser with two electro-opticalfeedback

3.2 Electro-optical device subjected to Nonlinear feedback pump current

3.2.1 The Model

In this section, we explore the effects of nonlinear feedback injected current on the laser as it is implemented through the setup exhibited in Fig.(3.12) where we can recognize the emitter. Here, the optical output of the Mach-Zehnder is now split into two parts using 2X2 fiber coupler: One part is detected by a photodiode which converts the optical light into electrical one with a sensibility s. After this operation, this electrical fraction of the signal is re-injected back in the active layer and therefore affects the stimulated emission dynamics of radiations in the laser which serves as a light source. The SC laser is therefore subjected to modulated feed-

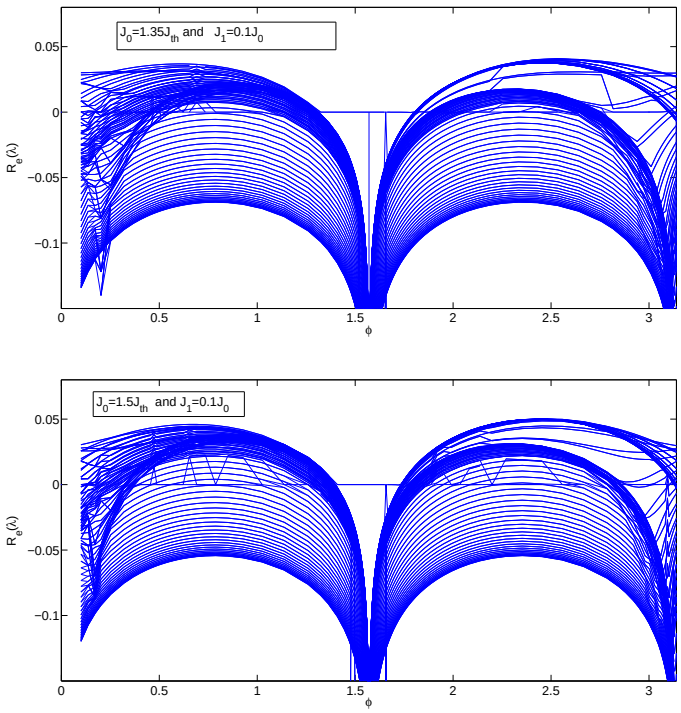

Figure 3.13: Real part of solutions given by the eigen equation versus off-set phase for $J_1 = 0.25J_0$

back pump current and the optical input of Mach-Zehnder is thereby related to it output. The second part of the signal crosses through the delay line, another photodiode and the linear filter which electrode is directly applied to the Mach-zehnder.

For the feedback loop, the equations remain unchanged whereas for the laser, we have

$$\frac{dI}{dt} = (G - \gamma)I \tag{3.10}$$

$$\frac{dN}{dt} = J_0 - \gamma_e N - GI + J_1 cos^2(X(t) + \phi) \tag{3.11}$$

where one notices the presence of the modulated extra-term coming from the modulated feedback pump current with the maximum value J_1 .

3.2.2 Theoretical and numerical study

The fixed point for this model is now (x_s, w_s, I_s, N_s) where
$x_s = 0$

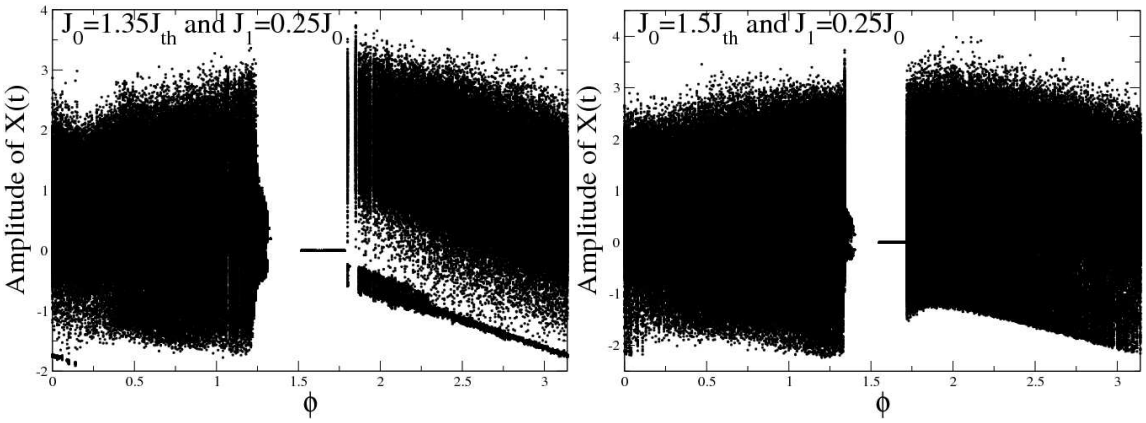

Figure 3.14: Bifurcation diagram versus off-set phase ϕ
for different injection current J_0

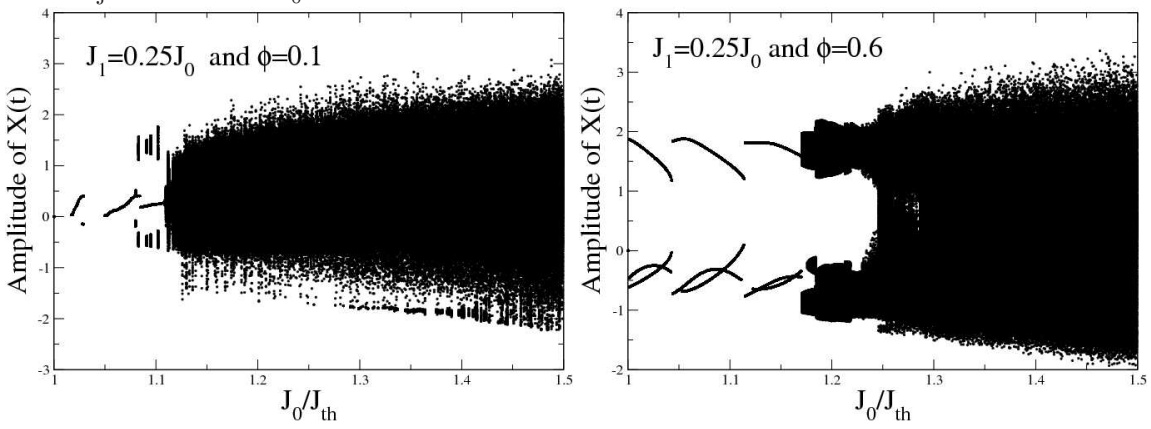

Figure 3.15: Bifurcation diagram versus injection current J_0
for different off-set phase ϕ

$w_s = \theta\beta_1 I_s \cos^2\phi$
$\mathrm{I}_{st} = \frac{(J_0+J_1 cos^2\phi)g_m - \gamma_e g_m N_0 - \gamma_e\gamma}{\gamma(g_m + s\gamma_e)}$
$N_{st} = \frac{g_m N_0 + \gamma + s(J_0+J_1 cos^2\phi)}{g_m + s\gamma_e}$

We can notice that with this mechanism the number of the photons at the steady state increases depending to DC component and bias electrode half-wave values of the Mach-Zehnder. Expanding the $cos^2(X(t)+\phi)$ terms in Fourier series around the fixed point, and taking into account only the first order terms, we find that the stability of the fixed point can be investigated through the eq.(3.2) where J_1 is shifted to $-J_1 sin2\phi$ ($J_1 \longrightarrow -J_1 sin2\phi$). We work with the parameters stated in Table 1 and 2 . Fig.(3.13) displays the stability analysis of the system using DDE-BIFTOOL algorithm in matlab with $J_1 = 0.25J_0$. We remark J_0 is that obtained without any feedback pump current. We notice that the predominated

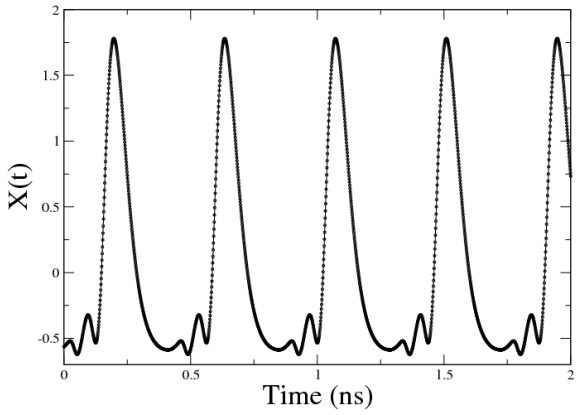

Figure 3.16: pulses generated with $J_0 = 1.01J_{th}$ and $\phi = \pi/4$.

zone of destructive effects remain only around $\pi/2$ with almost the same width as previously found.

Inspecting Fig.(3.14), we find that the feedback pump current induces more chaotic complexity of the carrier with respect to the phase and depending to the injection current. The implementation of nonlinear feedback pump current induces a variety of rich and complex behaviors of the system. First, the modulated injected current has an advantage that beyond the amplification of chaotic carrier, we can control the maximum injected back current which is J_1 and thereby avoid the large fluctuations which can destroy the laser.

In Fig.(3.15) we find that the presence of modulated injected current allows to generate instability even with the values of injected current closer to J_{th}. The value of J_{th} here is one obtained without any feedback injected current. With the value J_1 associated with appropriate pump current value J_0, the system generates more others rich behaviours. It is seen for instance that we can generate chaos from $J_0 = 1.15J_{th}$ for small phases ($\phi = 0.1$) or periodic behaviour with some ones ($\phi = \pi/4$). Among the periodic behaviours, we find the pulses plotted in Fig.(3.16) for $J_0 = 1.01J_{th}$ and $\phi = \pi/4$. Typically, we find that chaotic behaviour can be obtained for any phase (but those closer to $\pi/2$) using $J_0 \geq 1.25J_{th}$ which corresponds to the gain from about $\beta \geq 1.5$. Along the same line, one remarks that any chaotic behaviour becomes more chaotic independently of the off-set phase ϕ, and the injection current J_0 is added.

On the other hand, we can evaluate the effects of the feedback injected current

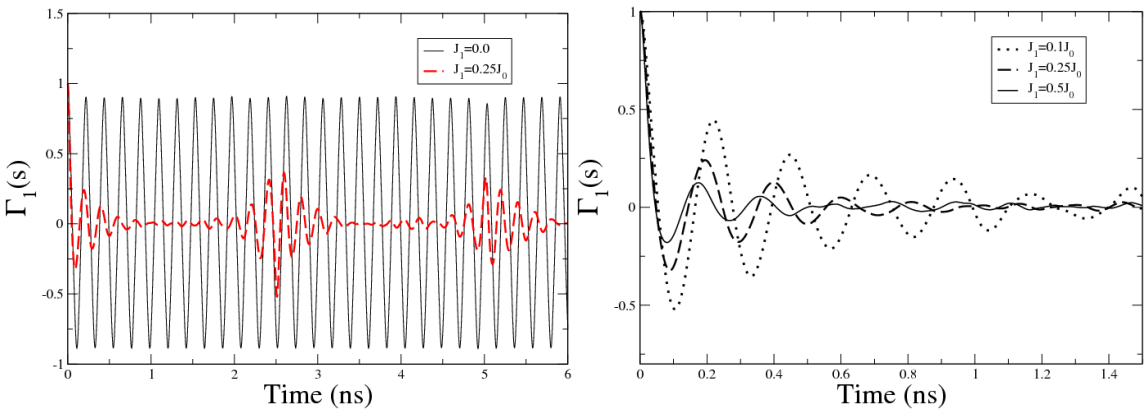

Figure 3.17: Auto-correlation function for different values of J_1

on the chaotic areas obtained without this latter feedback by comparing both carrier complexities ($J_1 = 0.0$ and $J_1 = 0.25J_0$). To meet this need, we plot in Fig.(3.17) the auto-correlation function for different values of the injected current. Fig.(3.17, left) confirms that the application of J_1 allows to have strong chaos from periodic oscillations since the correlation function decreases faster to zero when J_1 is applied. In addition, increasing the feedback pump current leads to faster decrease of the correlation function to zero shown in Fig.(3.17, right). Thus, further J_1 increasingly induces more chaotic complexity of the carrier.

Because the average of the feedback term in pump current is different to zero, it affects the laser gain which increases proportionally to $g_m J_1 cos^2\phi/(\gamma(g_m + s\gamma_e))$ which is the extra photon numbers at the steady state compared with one obtained without any feedback current. This term causes an increase of the gain parameter due to ϕ. With our parameters, the overall normalized gain is $\beta = 3.08$ witout any feedback pump currant and $\beta = 4.26$ with $J_1 = 0.25J_{th}$ and $\phi = \pi/4$ at the steady state. Nevertheless, the average of the overall optoelectronic gain is almost the same given at the steady state.

3.2.3 Synchronization of two electro-optical semiconductor lasers with two electro-optical feedbacks

As lately investigated, we consider two identical devices in the conditions described in section 2.3.1 with extra condition that the modulated injected current of the receiver is taken at the output of its Mach-Zehnder modulator. The emitter and

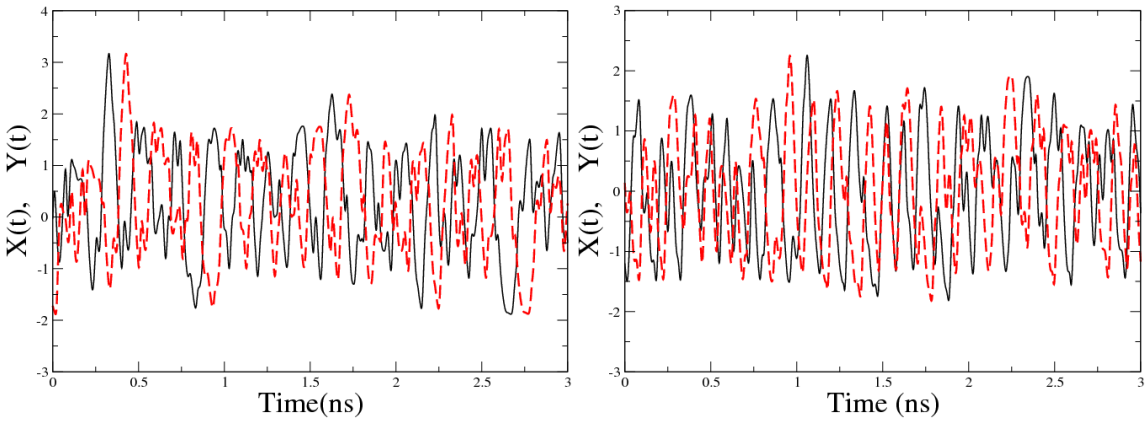

Figure 3.18: Emitter (solid line) and receiver (dashed line) time traces for $\Delta T = 0.1ns$ (left), and $\Delta T = -0.1ns$ (right). $J_0 = 1.5J_{th}$,$J_1 = 0.25J_0$ and $\phi = \pi/4$

receiver lasers are , respectively governed by

$$Emitter : \begin{cases} \frac{dI}{dt} &= (G-\gamma)I \\ \frac{dN}{dt} &= J_0 - \gamma_e N - GI + J_1 cos^2(X(t)+\phi) \end{cases} \tag{3.12}$$

$$receiver : \begin{cases} \frac{dI_s}{dt} &= (G_s-\gamma)I_s \\ \frac{dN_s}{dt} &= J_0 - \gamma_e N_s - G_s I_s + J_1 cos^2(y(t)+\phi) \end{cases} \tag{3.13}$$

assuming the same parameter for the master and slave. Fig.(3.18) shows synchronization of the master and slave when the injected pump current is modulated. Thus the model obeys the fundamental principles of synchronization in the same conditions as previously described.

3.2.4 Single parameter-mismatch

Fig.(3.19) displays the $J_1 - mismatch$ which embeds mismatch coming from the photodetector sensibility, as well as, coupler delay line. With this model, the feedback pump current coefficient J_1 has a minor effect on the synchronization since the correlation is still close to 1. Despite of this good correlation, the amplitude of the signal is affected by the mismatch since 1% mismatch generates 0.5% of synchronization error.

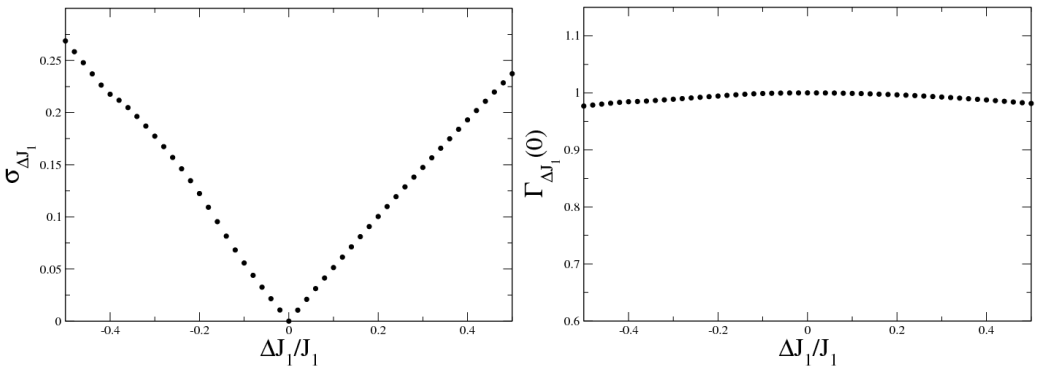

Figure 3.19: Average synchronization error at equal time (right) and maximum correlation (left) for J_1 mismatch

Fig.(3.20) confirms that J_1 has menor influence on the synchronization since there is only a slight difference between the model without and with modulated feedback injected current. Therefore , 1% of mismatch induces almost 1% of synchronization error in both cases while the correlation is still good even with large mismatch.

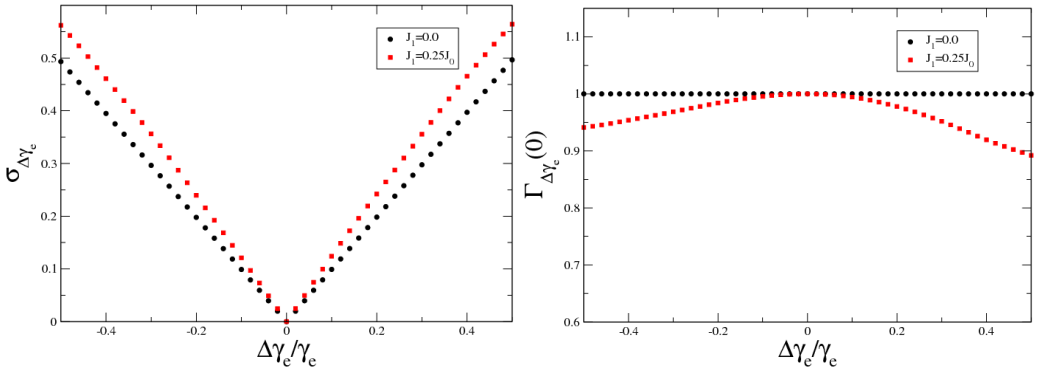

Figure 3.20: Average synchronization error at equal time (right) and maximum correlation (left) for γ_e mismatch

3.2.5 Encoded/Decoded message

We encode and recover the message using the mechanism shown in Fig.(3.12). The message can be recovered by subtracting off the chaos. Thus, using this process of recovery, we have:

$$S_c(t) = K^{'}(\beta_1 I \cos^2[x(t) + \phi] + \alpha m(t)) - K\beta_1 I_s \cos^2[y(t) + \phi_s] \tag{3.14}$$

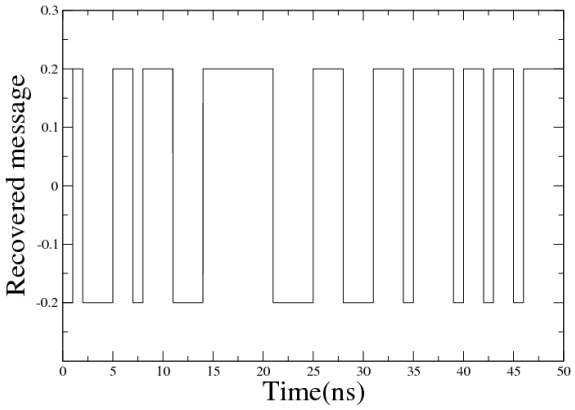

Figure 3.21: recovered message for $J_0 = 1.5J_{th}$, $J_1 = 0.25J_0$ and $\phi = \phi/4$

The analytical solution taking $x(t) = y(t)$ and $I(t) = I_s(t)$ and taking $k = k^{'}$ and $\phi_s = \phi$ leads to
$S_c(t) = K\alpha m(t)$
Fig.(3.21) shows the recovered message for $K = 1$ and $\alpha = 0.2$.

Chapter 4

Conclusion and future work

We have focused in this report on optical communications involving semiconductor laser with electro-optical feedback. This type of communications needed for confidential data transmission required chaotic complexity to scramble the message sent in public. This theory evolves many steps and the first one consists in generating the output power of the laser. To meet this need, the current is pumped in the active layer to induce photon emission which is necessary to obtain an optical power. We have shown that this technique predicts the laser to provide continuous waveform. By introducing the Mach-Zehnder modulator associated through the feedback loop, we have generated chaotic carrier complexity required for encryption and we have seen that, the chaos complexity increases with the injected current and also depends on the offset phase. However, we have found that, for some values of offset phase, the system leads to stationary state independently on the injected current.

On the other hand, we have described the processes guaranteeing the security and recovery of the encoded message. Thus, we have synchronized two chaotic carriers in which one is the emitter and other the receiver, unavoidable to the recovery process. The parameter mismatches have shown to be the key of the security for the model since we have proven that the mismatches should be small enough to guarantee high-quality synchronization required for the decryption of the message. The message has been encoded and decoded in the context of perfect synchronization.

This study has shown narrow spectra for most of the offset phases if the injected current is not high enough compared to the threshold current. To circumvent these drawbacks, a fraction of the signal has been taken in the feedback loop and injected back into the active layer of the laser. We have found in two different schemes that, this extra-feedback induces more complexity of the chaotic carrier. First, the situation has been explored by feeding back the laser with 10% of the pump current taken at the output of the filter. The properties of this extra-feedback on synchronization, and encoded/decoded message have found to be close enough to the previous device while the mismatch has shown to be more sensitive to the feedback

injected current mismatch. In the second scheme, 25% of the pump current taken at the output of the Mach-Zehnder modulator has also injected back in laser. In this last model, the synchronization, mismatches and encoded/decoded have shown quite similar to the results obtained without the feedback in laser.

The present work represents the development of reliable simulation and analytical analysis for this new model. Priority will devote in our future work to experimental implementation of these new models. The influence of the noise will be studied as well.

Bibliography

[1] Gilbert S. Vernam, Secret signaling system, U.S. Patent 1310719, (1919).

[2] B. Schneier, Applied Cryptography, 2^{nd}Edition,Wiley (1995).

[3] R. Rivest, A. Shamir, L. Adelman, Communications of the ACM 21, 120(1978).

[4] P. W. Shor, in Proc. of the 35^{th} Annual Symposium on Foundations of Computer Science,(IEEE Press) , 124 (1994).

[5] H. Haken,*Phys. Lett.* A 53, 77(1975).

[6] C. Bracikowski and R.Roy, Chaos 1, 49 (1991).

[7] M. V. Danileiko, A. L Kravchuk, V. N. Nechiporenko, A. M. Tselinko, and L. P. Yatsenko, "Dynamic chaos in a gas ring laser", Kvantovaya Elektron. (Moscow) 13, 2147-2149 (1986)

[8] Y. Choa and T. Umedaa, "Observation of chaos in a semiconductor laser with delayed feedback", Elsevier B.V., Volume 59, Issue 2, PP 131-136 (1986)

[9] L. M. Pecora and T. L. Carroll, " Synchronization in chaotic systems", Phys. Rev. Lett., vol. 64, no. 8, pp.821-824, (1990)

[10] K. M. Cuomo and A. V. Oppenheim, " Circuit implementation of Synchronized chaos with applications to communications", Phys. Rev. Lett., vol. 71, no. 1, pp.65-68, (1993)

[11] G. D. Van Wiggeren and R. Roy, " Communication with chaotic lasers",*Science* vol.279, pp. 1198-1200, (1998)

[12] G. D. Van Wiggeren and R. Roy," Chaotic Communications using Time delayed optical systems",*Int. J. of Bif. and chaos 9*, pp. 2129-2156, 1999

[13] C. R. Mirasso, P.Colet and P. García-Fernández, " Synchronization of chaotic semiconductors lasers: Application to Encoded communications", Phot. Tech. Lett. vol. 8, pp.299-301, (1996).

[14] A. Snchez-Daz, C.Mirasso, P. Colet and P. García-Fernández," Encoded Gbit/s Digital Communications with Synchronized Chaotic Semiconductor Lasers", IEEE J. Quantum Electron. 35, pp. 299-297, (1999)

[15] P. Spencer and C. R. Mirasso" Synchronization of Chaotic VCSELs", IEEE J. Quantum Electron. 35, pp. 803-809, (1999)

[16] H. F. Chen and J. M. Liu, " Open Loop Chaotic Synchronization of Injection Locked Semiconductor Lasers with Gigahertz Range Modulation ", IEEE J. Quantum Electron. 36, p.27, (2000).

[17] A. Uchida, M. Shinozuka, T. Ogawa and F. Kannari, " Experiments on Chaos Synchronization in Two Separate Microchip Lasers", Opt. Lett.vol. 24, pp890-892, (1999)

[18] U. M. Maurer: "Secret Key agreement by public discussion from commun information", IEEE Trans. Information Theory, Vol. 39 pp.733-742 (1993)

[19] J. Muramatsu, K. Yoshimura, K. Arai, and P. Davis: "Secret Key Capacity for optimally correlated sources under sampling attack", IEEE Trans. Information Theory, Vol. 52 pp.5140-5151 (2006)

[20] K. Ikeda, Opt. Commun. 30, 257 (1979)

[21] R. Lang and K. Kobayashi, IEEE J. Quantum Electron. 16, 347, (1980)

[22] P. Colet and R. Roy,*Opt. Lett.*. 19 (1994).

[23] G. D. Van Wiggeren and R. Roy, Science 279, 1198 (1998).

[24] G. Van Wiggeren and R. Roy, Phys. Rev. Lett. 81, 3547 (1998).

[25] L. Larger, J. P. Goedgebuer and F. Delorme, Phys. Rev. E 57, 6618 (1998).

[26] J. P. Goedgebuer, L. Larger, and H. Porte, Phys. Rev. Lett. 80, 2249 (1998).

[27] Y. Chembo Kouomou, P. Colet, N. Gastaud and L. Larger, Effect of parameter mismatch on the synchronization of semiconductor lasers with electrooptical feedback, Physical Review E 69, 056226 (2004).

[28] Y. Chembo Kouomou, P. Colet, L. Larger and N. Gastaud, Mismatchinduced bit error-rate in optical communications using semiconductor lasers with electro-optical feedback, IEEE Journal of Quantum Electronics, 41, 156 (2005).

[29] Y. Chembo Kouomou, P. Colet, L. Larger and N. Gastaud, Chaotic breathers in delayed electro-optical systems, Physical Review Letters 95, 203903 (2005).

[30] G. P. Agrawal and N. K. Dutta, "Long Waves Semiconductor Lasers", New York: Nostrand Reinhold, (1986).

[31] G. P. Agrawal, "Spectral hole burning and gain saturation in Semiconductor Lasers", J. Appl. Phys., vol. 63, pp. 1232-1234, (1988).

[32] P. Spano, A. D'Ottavi, B. Daino, and S. Piazzolla, "Experimental measurements and theory of first passage time in pulse-modulated Simiconductor Lasers", IEEE J. Quantum Electron., vol.25, pp.1440-1449 (1989).

[33] G. P. Agrawal, "Noise in Semiconductor Lasers and its impact in optical communication systems", In proc. SPIE. vol. 1376, R. Roy, Ed., pp. 224-235, (1990)

[34] V Z Tronciu1,2, Claudio R Mirasso1 and Pere Colet, "Chaos-based communications using semiconductor lasers subject to feedback from an integrated double cavity", J. Phys. B: At. Mol. Opt. Phys. 41 (2008)

[35] L. Larger, J. P. Goedgebuer, C. R. Physique 5 (2004).

[36] K. Engelborghs, T. Luzyanina, G. Samacy, Report TW 330, (2001)

[37] Shuo Tang and Jia-Ming Liu, "Effects of Message Encoding and Decoding on Synchronized Chaotic Optical Communications", IEEE J. QUANTUM ELECTRONICS, VOL. 39, NO. 11, (2003)

[38] J. G. Ford , M. G. Leonard , J. Swiss and G. C. Gainer "INSULDUR, IEEE Trans. Circuits Syst. I, vol. 49, pp. 163-169, (2002).